SYNTHESES AND OPTOELECTRONIC APPLICATIONS OF THIADIAZOLO QUINOXALINE BEARING ALTERNATING CONJUGATED COPOLYMERS

A THESIS SUBMITTED TO
THE GRADUATE SCHOOL OF NATURAL AND APPLIED SCIENCES
OF
MIDDLE EAST TECHNICAL UNIVERSITY

BY

EMRE ATAOĞLU

IN PARTIAL FULFILLMENT OF THE REQUIREMENTS
FOR
THE DEGREE OF MASTER OF SCIENCE
IN
POLYMER SCIENCE AND TECHNOLOGY

AUGUST 2016

Approval of the thesis:

SYNTHESES AND OPTOELECTRONIC APPLICATIONS OF THIADIAZOLO QUINOXALINE BEARING ALTERNATING CONJUGATED COPOLYMERS

submitted by **EMRE ATAOĞLU** in partial fulfillment of the requirements for the degree of **Master of Science in Polymer Science and Technology Department, Middle East Technical University** by,

Prof. Dr. Gülbin Dural Ünver _____
Dean, Graduate School of **Natural and Applied Sciences**

Prof. Dr. Necati Özkan _____
Head of Department, **Polymer Science and Technology**

Assoc. Prof. Dr. Ali Çırpan _____
Supervisor, **Department of Chemistry, METU**

Assoc. Prof. Dr. Emrah Ünalan _____
Co-Supervisor, **Dept. of Metallurgical and Materials Eng., METU**

Examining Committee Members:

Assoc. Prof. Dr. Gülay Ertaş _____
Chemistry Dept., METU

Assoc. Prof. Dr. Ali Çırpan _____
Chemistry Dept., METU

Assoc. Prof. Dr. İrem Erel Göktepe _____
Chemistry Dept., METU

Assoc. Prof. Dr. Yasemin Arslan Udum _____
Advanced Technologies Dept., Gazi University

Assist. Prof. Dr. Görkem Günbaş _____
Chemistry Dept., METU

Date: 24/08/2016

I hereby declare that all information in this document has been obtained and presented in accordance with academic rules and ethical conduct. I also declare that, as required by these rules and conduct, I have fully cited and referenced all materials and results that are not original to this work.

Name, Last name: EMRE ATAOĞLU

Signature:

ABSTRACT

SYNTHESES AND OPTOELECTRONIC APPLICATIONS OF THIADIAZOLO QUINOXALINE BEARING ALTERNATING CONJUGATED COPOLYMERS

Ataoğlu, Emre

M.S., Department of Polymer Science and Technology
Supervisor: Assoc. Prof. Dr. Ali Çırpan
Co-Advisor: Assoc. Prof. Dr. H. Emrah Ünalan

August 2016, 71 pages

Donor-acceptor type conjugated polymers containing thiadiazolo quinoxaline and benzodithiophene derivatives were used as photoactive material for organic solar cell. The alkoxy- substituted benzo[1,2-b;4,5-b']dithiophene (BDT) monomer, 2,6-bis(trimethyltin)-4,8-di(2-ethylhexyloxyl)benzo[1,2-b;4,5-b']dithiophene, was polymerized with 4,9-dibromo-[1,2,5]thiadiazolo[3,4-g]quinoxaline through a Pd(0)-catalyzed Stille coupling reaction. In order to improve the interchain interactions between polymer chains, an alkylthiophene-substituted BDT derivative was synthesized and polymerized with identical counter monomer. Chemically synthesized polymers were characterized by ^{1}H NMR, GPC, TGA and DSC. Electrochromic studies showed that polymers have similar multichromic properties. Both polymers have ocher color in their neutral states and grey color in their oxidized states. The lowest switching times obtained for both polymers were 0.9 s (975 nm) for **P1** and 1.0 s (425 nm) for **P2**. Optical band gap energies of **P1** and **P2** measured as 1.04 eV and 1.10 eV, respectively. Photovoltaic properties of the copolymers mixed [6,6]-phenyl

C71 –butyric acid methyl ester ($PC_{71}BM$), were investigated. **P2** exhibited the best device performance with an open circuit voltage of 0.52 V, short circuit current of 2.82 mA/cm^2 and power conversion efficiency of 0.73 % under Airmass 1.5 Global (AM1.5G, 100 mW/cm^2) illumination.

Keywords: Conjugated polymers, benzodithiophene, thiadiazolo quinoxaline, organic solar cells.

ÖZ

TİYADİAZOLO KİNOKZALİN TAŞIYAN ARDIŞIK KONJÜGE KOPOLİMERLERİN SENTEZİ VE OPTOELEKTRONİK UYGULAMALARI

Ataoğlu, Emre

Yüksek Lisans, Polimer Bilim ve Teknolojisi Bölümü
Tez Yöneticisi: Doç. Dr. Ali Çırpan
Ortak Tez Yöneticisi: Doç. Dr. H. Emrah Ünalan

Ağustos 2016, 71 sayfa

Tiyadiazolo kinokzalin ve benzoditiyofen türevi içeren donör- akseptör tipi konjüge polimerler organik güneş hüclerelerinde fotoaktif malzeme olarak kullanılmıştır. Alkoksi ikameli benzo[1,2-b;4,5-b']ditiyofen (BDT) monomeri, 2,6-bis(trimetiltin)-4,8-di(2-etil heksiloksi)benzo[1,2-b;4,5-b']ditiyofen, ve 4,9-dibromo-[1,2,5]tiyadiazol[3,4-g]kinokzalin Pd (0) katalizörü eşliğinde Stille kenetlenme reaksiyonu ile polimerleştirilmiştir. Polimer zincirlerinin birbirleri arasındaki etkileşimini arttırmak için alkiltiyofen yerleştirmeli BDT türevi sentezlenmiş ve aynı monomer ile polimerleştirilmiştir. Kimyasal olarak sentezlenen bu iki polimerin yapısal özellikleri ^{1}H NMR, GPC, TGA ve DSC ile aydınlatılmıştır. Ayrıca, elektrokromik çalışmalar polimerlerin benzer multikromik özelliklere sahip olduğunu göstermiştir. Her iki polimer de nötral hallerinde koyu sarı renge sahipken yükseltgendiklerinde gri renk göstermiştir. Anahtarlama zamanları **P1** için 0.9 s (975 nm) ve **P2** için 1.0 s (425 nm) olarak elde edilmiştir. **P1** ve **P2**'nin optik bant aralığı

sırasıyla 1.04 eV ve 1.10 eV olarak ölçülmüştür. [6,6] -fenil C71 -bütirik asit metil ester (PC71BM) ile karıştırılmış kopolimerlerin güneş pili özellikleri araştırılmıştır. **P2**, AM 1.5 G aydınlatma ortamında (100 mW/cm^2), 0.52 V açık devir gerilimi, 2.82 mA/cm^2 kısa devre akımı ve % 0.73 güç çevirim verimi özellikleri ile en iyi cihaz performansını göstermiştir.

Anahtar Kelimeler: Konjüge polimerler, benzoditiyofen, tiyadiazolo kinokzalin, organik güneş hücreleri.

To my beloved and family…

ACKNOWLEDGMENTS

I would like to thank my supervisor Assoc. Prof. Dr. Ali Çırpan for his endless and continues support and patience. Even if advisor- student relationship may be complicated entity consisting of advisor, counselor, boss, friend that can change in an instant I am sure that he was the only person that I can work during this period. It was a pleasure to work with him.

I would like to thank Prof. Dr. Levent Toppare for his guidance and support. His comments are priceless.

I also thank Assist. Prof. Dr. Görkem Günbaş for his scientific support. Most probably he is not aware of his help but I would like to specify that he always encouraged me when I was on the margin of withdrawal.

I would like to thank Naime Akbaşoğlu Ünlü, Hande Ünay and Ozan Erlik for accepting me and sharing their experiences in the very beginning of my study in B-47.

Several coworkers have had an important role in this study. Thanks go to Şerife Özdemir Hacıoğlu for electrochemistry studies and Gönül Hızalan for photovoltaic studies. I also appreciate the rest of the members of the Toppare group for being helpful when I needed it.

I also appreciate B47 members for those of them I had a chance to know during this study. They were always with me to overcome the worst days ever. Herein, I would like to present my thankfulness to all of them one by one. My time would not have been bearly as fun without their amity. Special thanks go to Şevki Can Cevher for being very kind and helpful. Words are not enough to describe my feelings to him.

I would like to express my gratitude to my parents for enduring my endless selfish acts during this study. I also want to thank my twin and elder brother to able to cheer me up and make finite moments meaningful.

The last but not the least, I do thank eternal sunshine of my life for her attempts to understand and encourage me during what has been simultaneously the most enjoyable and the most stressful part of my life. She made this study possible by helping me anytime. Without her love I could not be the person that I am now.

TABLE OF CONTENT

LIST OF TABLES

TABLES

LIST OF FIGURES

FIGURES

LIST OF ABBREVIATIONS

A	Acceptor
ACN	Acetonitrile
AM 1.5G	Air mass 1.5 Global
BDT	Benzodithiophene
BHJ	Bulk heterojunction
BLA	Bond length alternation
CB	Conduction band
CP	Conducting polymer
CV	Cyclic voltammetry
D	Donor
DSC	Differential scanning calorimetry
E_g	Band gap
E_g^{el}	Electronic band gap
E_g^{op}	Optical band gap
FF	Fill factor
HOMO	Highest occupied molecular orbital
HRMS	High resolution mass spectroscopy
GPC	Gel permeation chromatography
ITO	Indium tin oxide

I-PrOH	Isopropyl alcohol
J_{sc}	Short circuit current density
LUMO	Lowest unoccupied molecular orbital
NIR	Near infrared
NMR	Nuclear magnetic resonance
OPV	Organic photovoltaic
OSC	Organic solar cell
P_{max}	Maximum power
P_{in}	Power of the incident light
PA	Polyacetylene
PANI	Polyaniline
$PC_{71}BM$	[6,6]-Phenyl-C_{71}-butyric acid methyl ester
PCE	Power conversion efficiency
PEDOT	Poly(3,4-ethylenedioxy)thiophene
PPy	Polypyrrole
PSS	Polystyrene sulfonate
PT	Polythiophene
TGA	Thermogravimetric analysis
THF	Tetrahydrofuran
TLC	Thin layer chromatography
TMS	Tetramethylsilane
UV	Ultraviolet

V_{oc}	Open circuit voltage
VB	Valence band
Vis	Visible

CHAPTER 1

INTRODUCTION

1.1 Conducting Polymers

The discovery of that polyacetylene (PA) is highly electrically conductive upon doping with halogen vapor as iodine and bromine has led new field namely conducting polymers (CPs) at the end of 1970s [1]. PA is simplest linear conjugated polymer with a single chain structure (-CH=CH-) and each carbon is bounded to a hydrogen and two adjacent carbon atoms having sp^2 hybridization [2]. The field of conducting polymers which is also called as 'synthetic metals' was originally thought to be replaced to dense metals considering weight sensitive applications. Doped polyacetylene (PA) can compete with many metals in view of conductivity whereas its instability and insolubility with respect to bond alternation under ambient conditions restricts its practical use. Under the light of this unfortunate fact alternative CPs having superior stabilities was searched [3]. Even if the stability problem was solved with the discovery of non- degenerate polymers such as polyaniline (PANI), polypyrrole (PPy), polythiophenes (PTs), their conductivity was yet beyond PA [4]. After the discovery of PEDOT simple heterocyclic materials have largely been investigated due to their low band gap, compatibility and n-type doped ability [5]. The firstly synthesized polymers were shown in **Figure 1**.

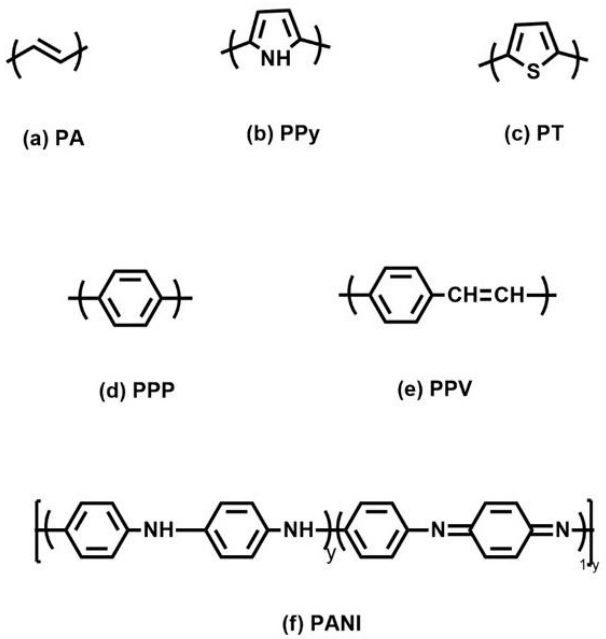

Figure 1. Firstly synthesized conducting polymers (a) polyacetylene; (b) polypyrrole; (c) polythiophene; (d) poly (p-phenylene); (e) poly (p-phenylenevinylene); (f) polyaniline

Combination of electrical properties of conductors with the plastics makes conducting polymers marvelous materials for technological application. The application field of conducting polymers varies from sensors to artificial muscles. Conducting polymers can be used to fabricate electronic devices as organic light emitting diodes (OLED), field emitting diodes (FEDs), organic field effect transistor (OFET) and organic solar cells (OSCs).

1.1.1 Doping Process

The transition of π- conjugated plastic from high band gap to very low band gap is carried out by 'doping' process [5]. The main idea in doping process for conducting polymers is withdrawing electron from polymeric chain (p-doping) or electron addition into polymeric chain (n-doping). The reaction of p- and n- doping using PA as example can be written as:

$[CH]_n + 3x/2 I_2 \rightarrow [CH]_n^{x+} + xI_3^-$ p-doping (oxidation with iodine)

$[CH]_n + xNa \rightarrow [CH]_n^{x-} + xNa^+$ n-doping (reduction with metal)

Doping process can be hatched matched and despatched through chemical or electrochemical method. For a conducting polymer solitons, polarons, bipolarons are proposed to understand increase in conductivity of conjugated polymers [1]. In general, soliton attends as charge transport for linear conducting polymer as PA [6]. On the other hand, polaron and bipolaron are used as charge carrier in non-degenerated conducting polymers [7]. Oxidation of heterocyclic conducting polymer creates a radical cation namely polaron. Similarly, further oxidation of this type of polymers creates bipolaron. Structures of soliton, polaron and bipolaran are represented in **Figure 2**. Due to the environmental limitations n- doped polymers are not common as p- doped polymers. Furthermore, both chemical and electrochemical have a drawback. When dopant ions in which they may be thought as charge stabilizer in conducting polymers were considered the process can result with structural deformation. Furthermore, this circumstance unfortunately decrease conductivity.

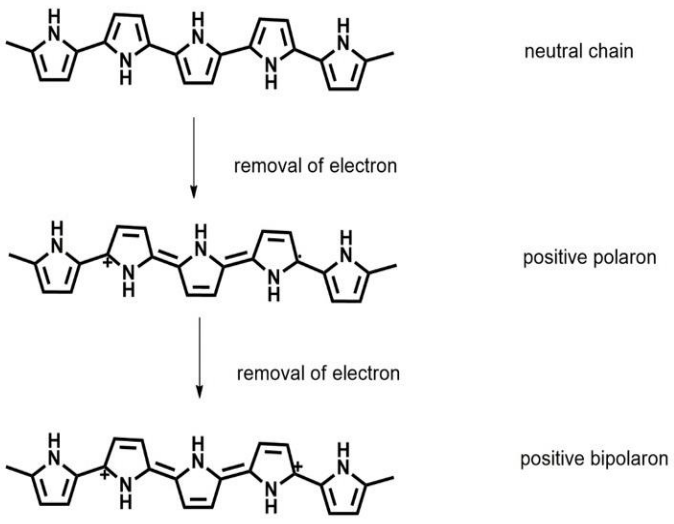

Figure 2. Representation of soliton, polaron and bipolaron

1.1.2 Band Gap Engineering

It is a trivial fact that for a material to be conductive, electrons should be able to excite from highest occupied molecular orbital (HOMO) to lowest unoccupied molecular orbital (LUMO). This methodology can be either photochemically or thermally [6]. In the determination of optical and electrical properties of a conjugated polymer the most important characteristic is the energy position of HOMO and LUMO energy levels and magnitude of band gap [8]. Depending on the nature of the material its band gap can be wide ($E_g > 3.0eV$), narrow or even zero.

In general, the optical band gap is determined by UV-Vis absorption and HOMO energy level is obtained using cyclic voltammetry if a polymer has only p- doping characteristic. Hence, LUMO energy level of the molecule can be calculated with a simple equation as $E_{LUMO} = E_{HOMO} + E^{opt}$. The narrower the band gap of the conjugated polymer leads to get high efficiencies from Bulk heterojunction solar cells [9]. For over a decade scientists try to design and control the band gap of semiconducting polymers since π-conjugated polymers allow limitless manipulations of their structures [6]. The easiest way to decrease band gap of the polymer is simply either lowering LUMO or enhancing HOMO level of the conjugated polymer. On the other hand, considering the device architecture dropping LUMO of the conjugated polymer may result with being lower LUMO level that of the fullerene. By doing that so might unfortunately block electron transfer significantly [10,11].

Moreover, even if it is stated that raising HOMO level of the conjugated polymer is a crucial way for efficient solar cell applications lifting HOMO level of conjugated polymer will result in loss of open circuit voltage. Since there are several critical prerequisites to obtain optimum band gap and so that developing the best match for solar output molecular engineering is crucial while designing conjugated polymer [6,12–14]. The methodologies namely aromaticity, bond length alternation, planarity, intermolecular influence and substitution directly affect the band gap of the π-conjugated conducting polymer [15]. In order to gain low band gap conjugated

polymer its resonance structure plays an important role. A conjugated polymer may have quinoid and aromatic form in their ground state. Quinoid form which is not energetically equivalent to its mesomeric form has higher energy thus lower energy gap. So that it can be said the higher the quinoid form of the material the lower in band gap. Moreover, there is a linear relationship between bond length alternation (BLA) and aromaticity. As the formation of quinoid structure increases on the backbone BLA starts to decrease. In addition, the energy difference between HOMO and LUMO energy level decreases when the substitution is added or enlarged on the backbone whilst the system starts to level of the number of chain exceeds a certain value which means substituent addition onto the monomer is limited for the reduction of band gap. This circumstance can be explained by the weak intermolecular interaction due to the bulk effect of long alkyl chain. Molecular orbital so that band gap can be tuned by incorporating electron- donating and electron- withdrawing substituents, which are basically the result of combination of resonance and inductive effects, onto aromatic ring in the backbone. HOMO energy level can be increased by introducing electron donating groups onto the backbone whilst electron withdrawing groups decrease the LUMO energy level of the material, arising a narrowed band gap. In literature, alkoxy group attached into an aromatic ring is mostly used as electron- releasing group. Likewise, nitro or cyano groups are preferred due to its electron- withdrawing ability resulting in decrease in LUMO energy level of the conjugated system. All of these parameters mentioned above are used to reduce band gap either by improving intermolecular interactions or by increasing π- conjugation length. On the other hand, applying these methods do not reduce the band gap extensively [15–17].

Through these various approaches towards the reduction of the bang gap of the conjugated system, donor- acceptor repeating unit strategy is the most efficient approach. In this donor- acceptor strategy electron deficient and electron rich moieties are used alternatively along the polymer backbone. In donor- acceptor type polymers the high energy level of HOMO of the donor and low energy level for LUMO of the acceptor results in low band gap because of intra- chain charge transfer from electron

rich moiety to electron deficient one and its schematic representation is depicted in **Figure 3**. This motivation which is reported by Hoeve and coworkers in 1993 provides to control not only band gap but also energy levels of the conjugated system. In the light of this information, large, medium and low band gap polymers can be synthesized from the combination of weak donor and acceptor, strong donor- weak acceptor (or vice versa) and strong donor and acceptor, respectively [14].

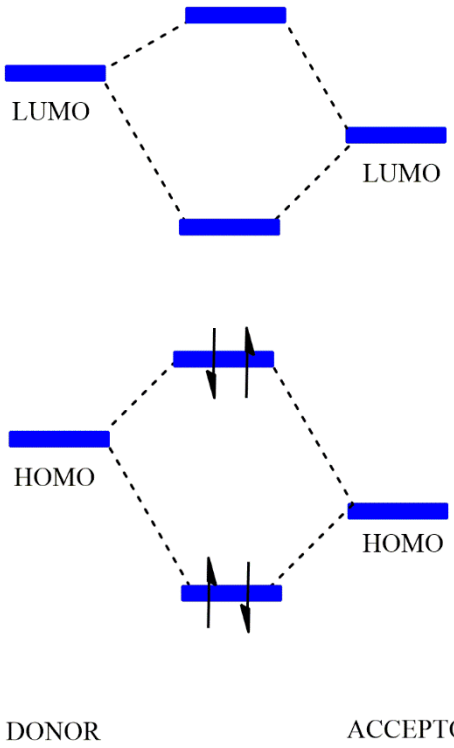

Figure 3. Interaction of donor acceptor moiety in D- A approach

1.1.3 Synthesis of Conjugated Polymers

Although there are plenty of polymerization methods the most commonly used and accepted ones are chemical polymerization and electrochemical polymerization. In chemical polymerization Stille coupling and Suzuki coupling are the most popular polymerization methods in the synthesis of conjugated polymers among Sonogashira coupling, Yamamato coupling, Tamao-Kumada-Corriu coupling [18].

In the synthesis of alternating and random copolymers Stille and Suzuki coupling reactions are the most efficient and widely used methods. In Stille coupling and Suzuki coupling palladium is used as catalyst due to its tolerance to mild conditions as well as variety of functional groups. Also, its characteristic mentioned above makes palladium catalyzed reactions more efficient compared to its parents such as lithium or Grignard reagents [19]. The cross coupling of reagents with organic electrophiles which is catalyzed by palladium is a promising method for carbon- carbon bond generation. It is noteworthy that stannyl group substituted on thiophene ring of the monomer is more suitable for Stille coupling reactions due to its high reactivity with aryl halides. Likewise, Suzuki coupling is extensively used for the synthesis of benzene containing polymers with boronic groups. The prerequisite of Suzuki coupling reaction is using a mild base as K_2CO_3. The reason of using such a base is basically boosting the reactivity of boronate anion. On the other hand, the noteworthy drawback of the Stille coupling reactions is the toxicity of stannylated monomers and its by-products. In Suzuki coupling reactions even if the reagents used in coupling are not toxic the primary obstacle is purification of monomers that contain boronic acid. In **Figure 4** schematic representation of Palladium-catalyzed cross coupling is shown. Although catalytic cycle is represented in Pd^0 to Pd^{II} oxidation state studies show that coupling reactions takes place via Pd^{II} to Pd^{IV} [6].

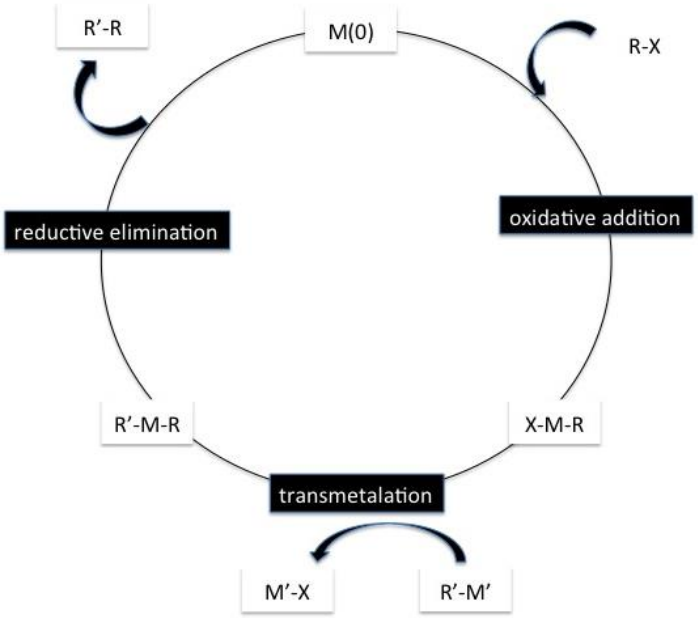

Figure 4. Schematic representation of palladium catalyzed cross coupling

In electrochemical polymerization monomers are oxidized onto the glass surface upon applied potential. The glass surface can be coated with indium tin oxide, platinum and gold. Even if the collected polymers on the electrode is small scale it gives very good information for further investigation as optical and electrochemical properties of the desired polymers. The most important thing in this method is the concentration of the monomer and type of electrode. The advantage of electropolymerization is ease of production, no need for further purification and rapidity.

The other method used in the synthesis of conjugated polymers is oxidative ferric chloride polymerization. The advantage of this method is no requirement of stannyl or halide group in monomer backbone. In general polymerization takes in place in 2- and 5- positions of the monomer containing hydrogen. The idea is that $FeCl_3$ initiates the oxidation of monomer to produce a radical center at the positions mentioned above predominantly which propagate to form polymer. In literature thiophene and its

derivatives are polymerized with $FeCl_3$. The major problem in $FeCl_3$ is that the method results with variable molecular weight even if the polymerization is repeated under identical conditions. The reason is different levels of iron impurities which directly change the molecular weight of the polymer. This method is preferred when high molecular weight polymer is required [19].

1.2 Organic Solar Cells

Organic solar cell (OSC) can be simply defined as the production of electricity from sunlight. The reason of being very popular for the last several decades is its ease of fabrication by large scale, low cost power production, solution processability and having a potential to be used in flexible substrates compared to inorganic one. However, I believe it is important to note that not having long- term stability and low performance compared with inorganic based solar cell are still the major problem that should be handled. Even if the most commonly used and accepted one is bulk heterojunction system considering device architecture some other types had been used as single layer and bilayer organic photovoltaics so far [20]. While using single layer organic photovoltaic cell the efficiency of the solar cell was monitored very low [21]. The reason of low efficiency of this type of solar cell lies in the architecture of the device. In this type the conjugated polymer is directly connected to the metal surface and the distance which is needed to dissociate the charges is very low. Since the exciton diffusion length is restricted about 10 nm the efficiency of single layer solar cell is very low [17,22,23].

On the other hand, different from the former one in bilayer organic solar cell structure there is a junction in which dissociation of the charges takes in place [8]. Even if the generated excitons are higher considering single layer structure exciton generation occurs only at the interface around 10- 20 nm between the donor and acceptor layer and the number of excitons accomplished the process is very low. Most of the generated excitons recombine and efficiency of the device drops drastically [22]. In bilayer structure rigid glass or polymer as PET is used as substrate and indium tin

oxide (ITO) is used as anode electrode. In order to overcome the diffusion length problem which directly affects the efficiency Yu et al. reported Bulk Heterojunction (BHJ) concept in 1995 for conjugated polymer based solar cell [24]. In bulk heterojunction system the synthesized conjugated polymer behave as donor and blended with fullerene (acceptor) derivative such as $PC_{60}BM$, $PC_{61}BM$ and $PC_{71}BM$. Here, it is important to note that [6,6]-Phenyl-C_{71}–butyric acid methyl ester ($PC_{71}BM$) is superior to [6,6]-Phenyl-C_{61}–butyric acid methyl ester ($PC_{60}BM$) [11]. The reason is that absorption of visible light is more efficient in former fullerene derivative. Blending donor and acceptor simply leads to generate electrical power before recombination process takes in place. At this point the most important thing that should be considered is the domain size of the conjugated polymer and PCBM. When the domains are large charge separation cannot be succeeded. In contrast small domains most probably leads to recombination of the separated charges. The optimum domain size of polymer and PCBM should lies in between 5 to 20 nm which is also the requirement range of exciton diffusion length. The other important parameter which directly influence the efficiency of the solar cell is the arrangement of the demanded donor and acceptor molecules. Morphology of the blended molecules should be in ordered structure so that photoexcited electron donor can transfer onto the fullerene. Moreover, the efficiency can be enhanced significantly by decreasing the thickness of the polymer: PCBM layer to an optimum value (100-200 nm) [12,25–30].

1.2.1 Working Principle of OSC

Bulk Heterojunction system was designed as the solution of exciton diffusion length problem in bilayer solar cell. In this device architecture soluble conjugated conducting polymer (acting as electron donor) and fullerene derivative (having an electron affinity that is higher than the electron affinity of synthesized polymer) are blended with a typical size of tens of nanometers in the film. In general the operation of solar cell comprised of four main stages. Firstly, the incident photon with an energy ($E=h\upsilon$) is absorbed by polymer (donor) in active layer, secondly, generation of electron and hole

pair which is called exciton, diffusion of the generated excitons onto the donor-acceptor interface. When exciton diffuses to the donor- acceptor interface in which heterojunction is created with two different organic materials with a suited alignment. This circumstance leads to photoinduced charge transfer which is so called dissociation of excitons into electron and hole helding with Coulombic attraction. As a result of photoinduced charge transfer separated charges are collected in the corresponding counterparts. Holes are collected in anode compartment (ITO) and electrons are transported onto cathode compartment [10,31–33].

1.2.2 Fabrication and Characterization of Bulk Heterojunction Cells

In Bulk Heterojunction Cells the blended semiconducting donor and acceptor molecules are sandwiched between two electrodes. The device is built on a transparent substrate. The ordinary conventional device architecture is composed of indium tin oxide (ITO) on glass substrate polyethylenedioxythiophene: polystyrene sulfonate (PEDOT: PSS) photoactive blend layer and a metal (usually aluminum used as cathode). ITO which behaves as anode allows light pass through and collects holes from the device. PEDOT: PSS which is used as hole transport layer is spin coated on top of the ITO coated glass substrate in order to ease capturing of holes. Also its role is attending exciton blocker. The reason of spin coating of PEDOT: PSS is to get smooth surface and increasing the work function of the electrode by sealing the active layer from ambient atmosphere. Also, its transparent properties in the visible and near IR region makes ITO and PEDOT: PSS better candidate for device structure. In order to obtain desired film thickness and quality the blended photoactive conducting material is spin coated from a common solution with various speed onto PEDOT: PSS surface. In literature aluminum which serves as cathode is most widely used metal in solar cell applications among calcium and silver. Although calcium electrode gives higher open circuit voltage (V_{oc}) compared to aluminum having lower work function and easily oxidized properties push calcium into the background. In order to have efficient charge transfer organic molecules' work function must match with the work

function of indium tin oxide (4.7 eV) and aluminum (4.3 eV). Aluminum in which its function is to collect electrons from the device is thermally evaporated with a thickness of 100 nm which is optimum thickness in order to get efficient solar cell. LiF is also evaporated to optimize the work function of cathode. Moreover, in order to overcome the device lifetime of conventional BHJ organic solar cell, inverted BHJ device was developed. In this architecture, the system composed of ITO/ electron transport layer/ active layer/ hole transport layer/ metal. ZnO which is coated onto ITO substrate is generally used as electron transport layer. Moreover, on top of that fullerene derivative and conjugated polymer is blended. The reason of using ZnO is to collect electrons selectively. Besides that, MoO_x is installed between active layer and metal to gather holes. Ag which has high work function is generally employed instead of Al. Basic organic solar cell device configuration is shown in **Figure 5**.

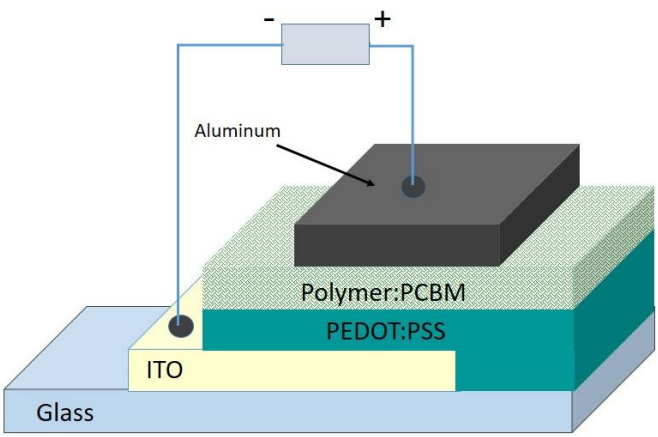

Figure 5. Representation of organic solar cell device configuration

1.2.3 Parameters Influencing Device Characteristics for OSCs

The characterization of OSCs are performed under the lighting of AM 1.5G solar spectrum. Organic solar cell's power conversion efficiency (PCE) is determined using three parameters namely open circuit voltage (V_{oc}), short circuit current density (J_{sc}) and fill factor (FF). All the parameters are shown in **Figure 6**. The relationship of these

parameters are demonstrated in Figure 5. Power conversion efficiency of a device can be calculated using equation

$$\eta_e = \frac{JscVocFF}{Pin}$$

in which P_{in} is incident light power on the device, V_{oc} is open circuit voltage, J_{sc} is short circuit current and FF is fill factor.

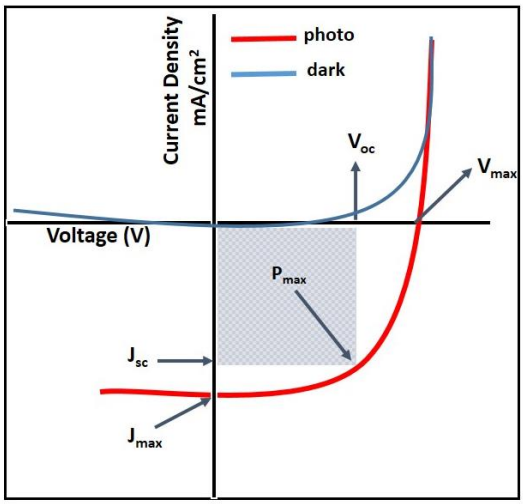

Figure 6. Current- voltage curve in dark and under illumination

1.2.3.1 Open Circuit Voltage

Yet, in bulk heterojunction devices the origin of open circuit voltage is not fully understood it is basically implied as electrical potential difference between two terminals when a device is not connected to any circuit. In 2001, Brabec et al. proposed that V_{oc} is directly related with the HOMO level of the conjugated polymer and LUMO level of the fullerene derivative. To illustrate, using an electron acceptor with a higher LUMO level than PCBM open circuit voltage of polymer solar cell can be improved efficiently. Similarly, using electron donor with deeper HOMO level will result in increase in V_{oc} of the PSCs. Also, it is stated there is linear relationship between

electron affinity of fullerene and V_{oc}. The type of metal used as cathode is weakly dependent to obtain high V_{oc}. In 2006, Scharber et al. derived an equation for the device to calculate V_{oc} theoretically as;

$V_{oc} = (1/q) [E_{HOMO}^{donor} - E_{LUMO}^{acceptor}] – 0.3$ V where,

q is elementary charge

E_{HOMO}^{donor} is HOMO energy level of the donor

$E_{LUMO}^{acceptor}$ is LUMO energy level of the acceptor

1.2.3.2 Short Circuit Current Density

Short circuit current density which is directly related with external quantum efficiency can be defined as the generation of current when there is not any external potential applied. The external quantum efficiency is the ratio of number of generated electrons under short circuit conditions to the number of incoming photons. Decreasing the band gap of the donor material significantly increase short circuit current density. Moreover, the value of short circuit current primarily depends on charge carrier mobility of the conjugated polymer.

1.2.3.3 Fill Factor

Fill factor play a crucial role in the determination of quality of photovoltaic device. Considering the recombination of exciton in donor- acceptor interface fill factor deviates from the ideal value of 1. FF can be formulated as;

$$FF = \frac{J_{max}V_{max}}{J_{SC}V_{OC}}$$

Fill factor is determined with charge carriers arriving the electrodes when the built- in field is lowered toward V_{oc}. Moreover, the series resistances affect the filling factor drastically and that should be minimized. Furthermore, the limited conductivity of ITO substrate limits the FF when solar cell is fabricated on large area. The device also

should not demonstrate ‘short’ between electrodes in order of maximizing the parallel shunt resistance.

1.2.4 Donor Materials’ effect in Organic Solar Cell Fabrication

In order to develop power conversion efficiency of polymer solar cells (PSCs) many research groups dedicated to the synthesis and design of polymeric donor units. The key requirements to get highly efficient conjugated polymer which behaves as donor in fabrication of BHJ organic solar cell are narrower energy band gap, higher hole mobility, relatively lower lying LUMO and broad absorption of the solar spectrum. All these requirements are not independent from each other. In order to harvest sun light efficiently donor material should have strong and broad absorption in near infrared and visible region (generally at around 700 nm). If it is succeeded short-circuit current will increase. Moreover, in order to obtain high charge separation, the alignment of HOMO and LUMO should be suitable. Another requirement is having high lying HOMO energy level of donor material to enhance open circuit voltage. Here, it is important to note that the mismatch of the absorption of the polymer solar cells and the solar irradiance spectrum is the fundamental obstacle in accomplishing high PCE [16]. The reason of importance of high charge carrier mobility is its crucial role in recombination process. Donor moiety having high charge carrier mobility helps to minimize recombination and promote charge transport efficiency which leads to get high fill factor and short circuit current. Furthermore, donor moiety should have suitable morphology to get effective charge separation [12].

1.3 Donor Units in Polymer Backbone

Electron rich compounds can be classified as weak, medium and strong according to their donating ability. Dibenzene containing donor units generally reveal weak donor ability due to its electron deficient nature. Even if it is mentioned previously that tuning the band gap of the polymer is possible with molecular modifications benzene containing donor units usually exhibit large band gap and poor light absorption. On

the other hand, dithiophene bridged donor moieties exhibit too strong donor ability and planarity due to its powerful electron delocalization feature. In spite of that, combination of thiophene and benzene units discover both units' characteristics. Their coplanar geometry enlarges π- electron delocalization [28]. In **Figure 7** basic donor unit's structures are shown.

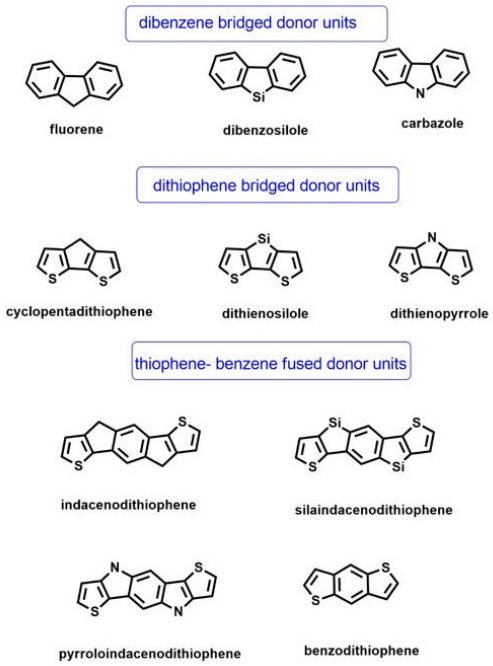

Figure 7. Commonly used donor units

1.4 Acceptor Units in Polymer Backbone

Electron deficient units mostly contain carbonyl or imine groups in their backbone. Acceptor units can also be divided into three part as weak, medium and strong according to electron withdrawing ability. Benzobisthiazole which is used widely in literature can be considered as weak acceptor. Besides that, benzotriazole is very good example for average electron acceptor. Furthermore, benzothiadiazole and quinoxaline

is commonly used acceptor units in order to get low band gap polymers [28]. Mostly used acceptor units' chemical structures are depicted in **Figure 8**.

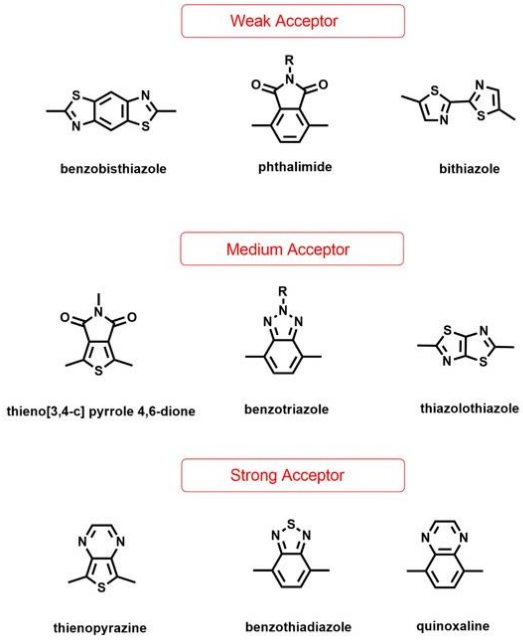

Figure 8. Acceptor units in polymer backbone

1.5 Moieties Used in This Study

1.5.1 Quinoxaline Based Conjugated Polymers

Quinoxaline based conjugated polymer series was firstly synthesized by Kitamura et al. in 1995 [34]. The lowest band gap containing quinoxaline was reported as 0.5 eV [35]. Its quinoid-acceptor feature makes quinoxaline bearing conjugated polymer good candidate for low band gap polymers. Quinoxaline is a typical electron deficient unit due to having two nitrogen atoms which is highly electronegative in the structure [36]. In this type of polymers relaxation of bond length alternation plays an important role to ease charge separation [36,37]. Also, its high electron affinity, low ionization potential and planarity features lead to be used in lots of applications in organic solar cells (OSC), organic light emitting diodes (OLED), organic field effect transistors (OFET) [38–40]. Furthermore, these units' electron affinity and ionization potential

characteristics enhance charge transport at moderate potentials in photovoltaic devices which leads an increase in efficiency [39]. In literature quinoxaline bearing conjugated polymers exhibit PCE of 2-6% [37]. Thiadiazoloquinoxaline unit which is subunit of quinoxaline moiety has been reported to have bang gap 0.90- 1.5 eV depending on the power of the donor unit and bulkiness of the side groups used in acceptor unit. On the other hand, unfortunately due to the lack of solubility and poor thin film morphology the efficiency of the polymers containing this subunit generally reveal under 1.0% PCE [41,42]. Quinoxaline containing conjugated polymers are depicted in **Figure 9**.

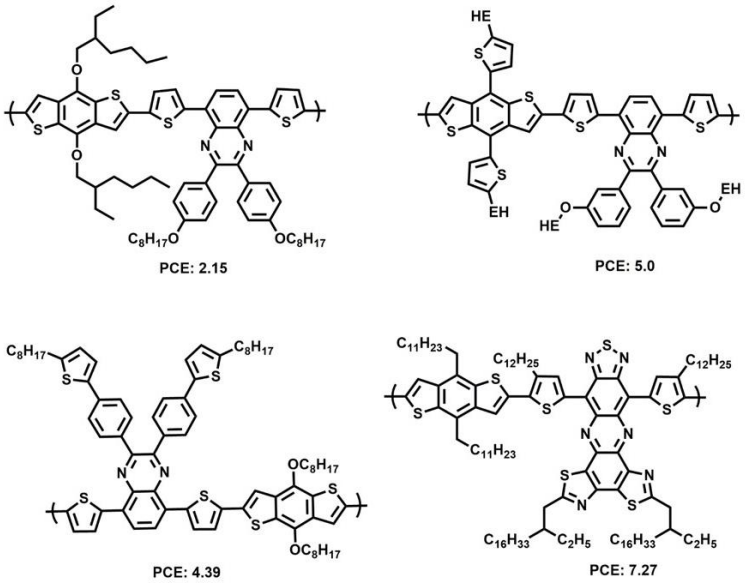

Figure 9. Examples of quinoxaline bearing conjugated polymers

1.5.2 Benzodithiophene Based Conjugated Polymers

Recently, benzo(1,2-b:4,5-b')dithiophene (BDT) bearing conjugated polymers have been flame up as an attractive electon rich component for solar cell applications due to its two important advantages. One is the BDT unit manage to maximize the π- orbital overlap by restricting intermolecular rotation. That characteristic of BDT furthermore, facilitate charge transport through intermolecular hopping. The other advantage is its structure. The BDT unit leads the polymer backbone to be more rigid and coplanar so

that efficient π-conjugation is succeeded [43,44]. Moreover, this results in lowering the band gap by raising HOMO energy level and broadening the absorption band gap. In comparison with the other mostly used conjugated building blocks as thiophene and thienothiophene BDT based polymers have relatively better balance between HOMO level and band gap [45]. The possibility of side group manipulation for good solubility and processability makes BDT highly preferred donor unit [46–48]. In the reported works BDT is mostly functionalized with side groups as alkoxy, alkyl and alkylthienyl on the 4- and 8- positions in order to get solution processable polymers [45]. In literature introducing aromatic ring into BDT unit on the 4- and 8- positions is identified as two- dimensional (2-D) conjugated structure of BDT. Studies reveal that introducing thiophene unit at the 4- and 8- positions of the BDT unit enhances conjugation and interchain interactions between polymers chains and so that higher J_{sc} can be achieved. BDT with two- dimensional conjugated structure exhibit broad and strong absorption bands owing to an extended side chain [46].

Moreover, in order to improve the solubility and impact the photovoltaic performance positively alkyl chain substituents are employed on the thiophene unit which is so called alkylthienyl- substituted BDT. Studies also reveal that using conjugated thiophene side chain leads to relatively high hole mobility which results with an increase in V_{oc} [49–51]. Moreover, 2-D conjugated BDT units have higher conjugated planes than their one- dimensional counterparts do. The reason it that the former one helps to form better inter-chain π-π overlapping [46,52]. Some BDT containing conjugated polymers performing over 5 % power conversion efficiency are depicted in **Figure 10** and **Figure 11** [45,52–54].

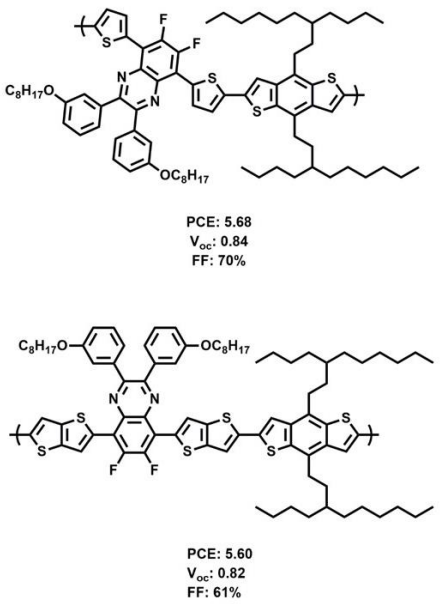

Figure 10. BDT and quinoxaline containing conjugated polymers

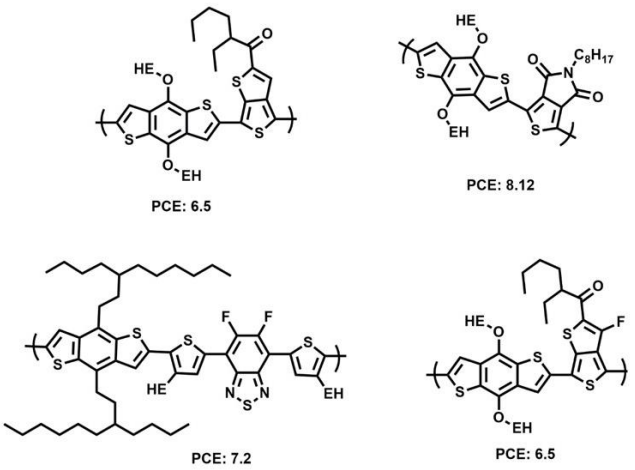

Figure 11. Examples of BDT containing conjugated polymers

1.5.3 Aim of the Study

Thiadiazoloquinoxaline units having four imines in the structure are commonly used in polymer backbone as an acceptor unit. In literature low band gap polymers was obtained using this subunit as an acceptor due to its strong electron withdrawing

properties which leads to decrease in LUMO level. Considering outstanding electron affinity of thiadiazoloquinoxaline with its ability to adopt quinoid form and variable chemical structures makes these polymers popular. Moreover, benzodithiophene with its symmetric and planar structure is widely used as electron rich unit in conjugated polymer engineering. In this study, our aim was to combine these remarkable and unique properties of each unit to obtain high efficiencies in organic solar cell applications. As indicated previously, besides attaching electron rich and electron deficient side group alternatingly, designing conducting polymer with stabilized quinoid structures is proved to be effective to reduce band gap. For this purpose, thiadiazoloquinoxaline and benzodithiophene bearing conjugated polymers were designed and synthesized based on this strategy via Stille polycondensation reaction. The synthesized polymers based on benzodithiophene and thiadiazoloquinoxaline with an identical backbone but different side groups attached at 4 and 8 positions of their benzodithiophene units were shown in **Figure 12**. Since thiadiazoloquinoxaline units exhibit low solubility, alkoxy substituent was attached onto electron deficient unit. Introduction of alkoxy group onto thiadiazoloquinoxaline unit shifts HOMO/LUMO energy levels with subsequent lowering band gap [6]. Moreover, the alkoxy substituents have profound effects on their charge transfer abilities and film forming properties. Furthermore, as it is stated above, benzodithiophene containing π-conjugated systems are widely used due to its coplanar structure which increase π-electron delocalization. Using cyclic voltammetry optical and electrochemical studies were investigated. Chemically synthesized alternating conjugated polymers were used as donor in photovoltaic devices with [6,6]-phenyl-C_{71}-butyric acid methyl ester (PCBM) as the acceptor.

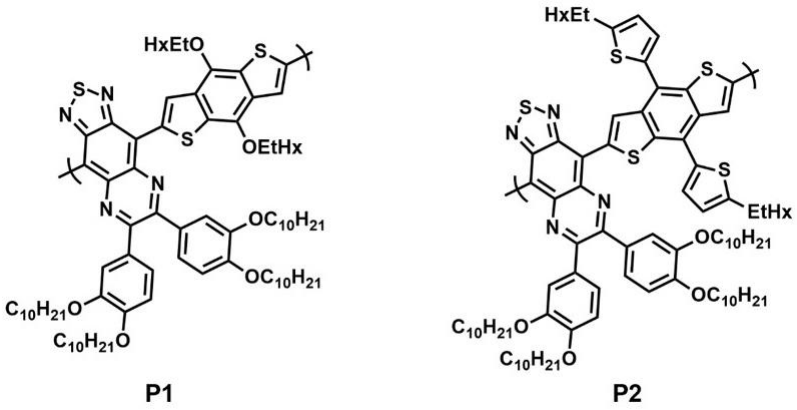

Figure 12. Synthesized polymers in this study

CHAPTER 2

EXPERIMENTAL

2.1 Materials and Equipments

All chemicals used in the synthesis were purchased from Sigma- Aldrich Chemical Co. Ltd. and they were used without any further purification. $PC_{71}BM$ was supplied from Solenna. Crude toluene and tetrahydrofuran (THF) were dried via sodium and benzophenone ketyl and distilled solvents were freshly used in the reactions. All reactions were carried out under protected atmosphere with argon unless otherwise mentioned. Crude materials were purified using Silica Gel 60 which is supplied from Merck. Structures were characterized via nuclear magnetic resonance (NMR) in deuterated chloroform which is used as reference solvent. Chemical shifts in the structure were reported in ppm at 7.26 and 77 ppm by taking tetramethylsilane as internal reference for ^{1}H and ^{13}C, respectively. Synthesized polymers' UV-Vis spectra were monitored at ambient temperature via Varian Carry 5000 UV-Vis spectrometer. Using Gel Permeation Chromatography (GPC) molecular weights of the polymers were recorded. In GPC polystyrene and chloroform were used as stationary phase and mobile phase, respectively. By using GAMRY Reference 600 potentiostat cyclic voltammetry studies were carried out for the polymers. In order to determine the molecular weight of the donor moiety high resolution mass spectroscopy (HRMS) technique was used. Thermal characteristic of the polymers was investigated by thermal gravimetric analysis (TGA) under nitrogen atmosphere. Heat flow of the

synthesized polymers with respect to temperature was monitored using Differential Scanning Calorimetry (DSC) technique under N_2 atmosphere.

2.2 Synopsis of Synthetic Procedures

2.2.1 Synthesis of 4,7-dibromobenzo[c][1,2,5]thiadiazole

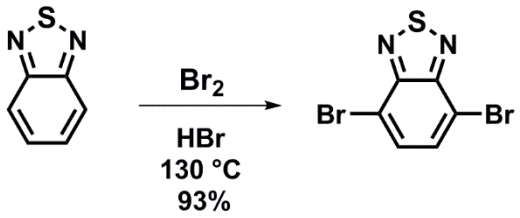

Figure 13. Synthesis of 4,7-dibromobenzo[c][1,2,5]thiadiazole

Benzo[c][1,2,5]thiadiazole (2.0 g, 14.7 mmol) was dissolved in 250 mL of two necked round bottom flask with 60 mL of 47% HBr at room temperature. Then Br_2 (7.1 g, 44.1 mmol) was added dropwise into the solution at ambient temperature. The solution was refluxed for about 6 hours at 130 °C. The mixture containing yellow solid was allowed to cool room temperature. The excess bromine and hydrobromic acid containing solution was filtered and then crude material was washed with $NaHSO_3$ (3x250mL) in order to consume bromine in filter. The filtrate was further washed with cold diethylether (3x250mL). The filtrate was dried and a yellow solid was obtained (4.0 g, 93% yield) [55].

^{1}H NMR (400 MHz, $CDCl_3$) δ 7.73 (s, 2H).

^{13}C NMR (101 MHz, $CDCl_3$) δ 152.97, 132.36, 113.92.

2.2.2 Synthesis of 4,7-dibromo-5,6-dinitrobenzo[c][1,2,5]thiadiazole

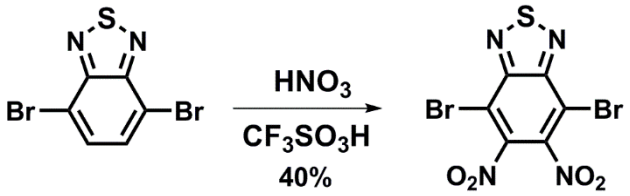

Figure 14. Synthesis of 4,7-dibromo-5,6-dinitrobenzo[c][1,2,5]thiadiazole

4,7-dibromo-5,6-dinitrobenzo[c][1,2,5]thiadiazole was synthesized as indicated in literature [56]. Fuming HNO_3 (1.5 g, 23.8 mmol) was added dropwise into two necked round bottom flask containing CF_3SO_3H (10.0 g, 66.7 mmol) at 0 °C. Just after the addition of fuming HNO_3 insoluble complex produced immediately. 4,7-dibromobenzo[c][1,2,5]thiadiazole (2.5 g, 8.6 mmol) was added to the mixed acid in portions over 20 min keeping the temperature below 5 °C . After 2 hours, the mixture was let to warm 50 °C and stirred overnight. The mixture was poured into 500 mL of ice cold and the product was precipitated. The precipitate was filtered and the desired product was obtained as light yellow powder after recrystallization from ethanol (1.3 g, 40% yield).

2.2.3 Synthesis of 4,7-dibromobenzo[c][1,2,5]thiadiazole-5,6-diamine

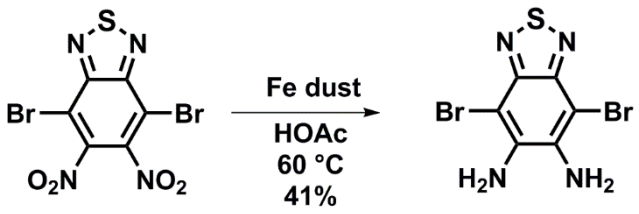

Figure 15. Synthesis of 4,7-dibromobenzo[c][1,2,5]thiadiazole-5,6-diamine

4,7-dibromobenzo[c][1,2,5]thiadiazole-5,6-diamine was synthesized as indicated in literature [57]. Firstly, iron powder was treated with 1.0 M HCl, ethanol and ether, respectively. Then Fe powder (1.0 g, 17.8 mmol) was put into 50 mL of two necked

round bottom flask containing 10 mL acetic acid. 4,7-dibromo-5,6-dinitrobenzo[c][1,2,5]thiadiazole (0.56 g, 1.46 mmol) was added portionwise and then the mixture was heated to 60 °C. Completion of reaction was determined by TLC. Reaction was cooled to room temperature and the formed precipitate was filtered. Crude material was taken with hot ethyl acetate and filtered to get rid of any remaining iron powder. Evaporation of solvent followed by recrystallization from ethanol gave pale yellow solid which was used without any further purification (195 mg, yield 41%).

2.2.4 Synthesis of 1,2-bis(decyloxy)benzene

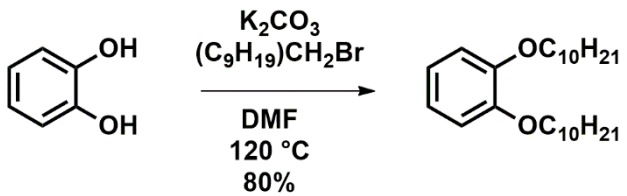

Figure 16. Synthesis of 1,2-bis(decyloxy)benzene

In an argon purged 250 mL of two necked round bottom flask pyrocatechol (6.0 g, 54 mmol) and anhydrous potassium carbonate (22.8 g, 162 mmol) were dissolved into N,N-dimethylformamide (40 mL) After 30 min., 1-bromodecane (27.8 g, 125 mmol) was added slowly and the reaction mixture was stirred at 120 °C. Completion of reaction was determined by TLC. The reaction was cooled down to ambient temperature and the solvent was evaporated. The residue was dissolved in dichloromethane and washed with water three times. Solvent was evaporated and purification was performed using column chromatography (hexane:DCM 2/1). White solid product was obtained with after precipitation from methanol (10.9 g, yield 80%) [58].

^{1}H NMR (400 MHz, $CDCl_3$) δ 6.93 – 6.80 (s, 4H), 3.99 (t, J = 6.7 Hz, 4H), 1.86 – 1.77 (m, 4H), 1.47 (td, J = 15.4, 8.1 Hz, 4H), 1.38 – 1.21 (m, 28H), 0.88 (t, J = 6.8 Hz, 6H).

2.2.5 Synthesis of 1,2-bis(3,4-bis(decyloxy)phenyl)ethane-1,2-dione

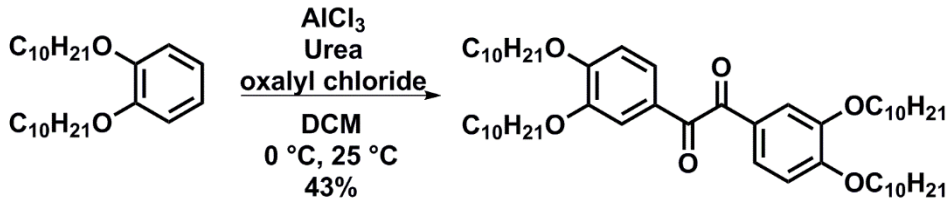

Figure 17. Synthesis of 1,2-bis(3,4-bis(decyloxy)phenyl)ethane-1,2-dione

In a two necked bottom flask 1,2-bis(decyloxy)benzene (500 mg, 1.28 mmol), urea (73.0 mg, 1.21 mmol) and $AlCl_3$ (257 mg, 1.93 mmol) were dissolved in 10 mL of DCM under argon atmosphere at 0 °C. Oxalyl chloride (50 mg, 0.64 mmol) was added dropwise into reaction mixture at 0 °C and the reaction was let to warm to room temperature. The mixture was stirred overnight at ambient temperature. The brown suspension was poured into cold water. Organic phase was separated and the aqueous phase was extracted with DCM. Then the combined organic phase were washed with $NaHCO_3$ solution. Organic phase was dried over $MgSO_4$ and evaporated in rotary. Column chromatography on silica gel was carried out with hexane and DCM (1:2) as the eluent. Further purification was performed by precipitation using methanol to obtain a milk white solid (230 mg, 43% yield) [59].

^{1}H NMR (400 MHz, $CDCl_3$) δ 7.57 (d, J = 1.9 Hz, 2H), 7.43 (dd, J = 8.4, 1.9 Hz, 2H), 6.84 (d, J = 8.5 Hz, 2H), 4.05 (td, J = 6.6, 1.9 Hz, 8H), 1.88 – 1.79 (m, 8H), 1.50 – 1.41 (m, 8H), 1.27 (s, 52H), 0.88 (dt, J = 7.0, 3.3 Hz, 12H).

^{13}C NMR (100 MHz, $CDCl_3$) δ 193.8, 155.0, 149.35, 126.1, 69.1, 31.9, 29.6, 29.3, 29.1, 28.9, 26.0, 25.9, 22.7, 14.1.

2.2.6 Synthesis of 6,7-bis(3,4-bis(decyloxy)phenyl)-4,9-dibromo-[1,2,5]thiadiazolo[3,4-g]quinoxaline

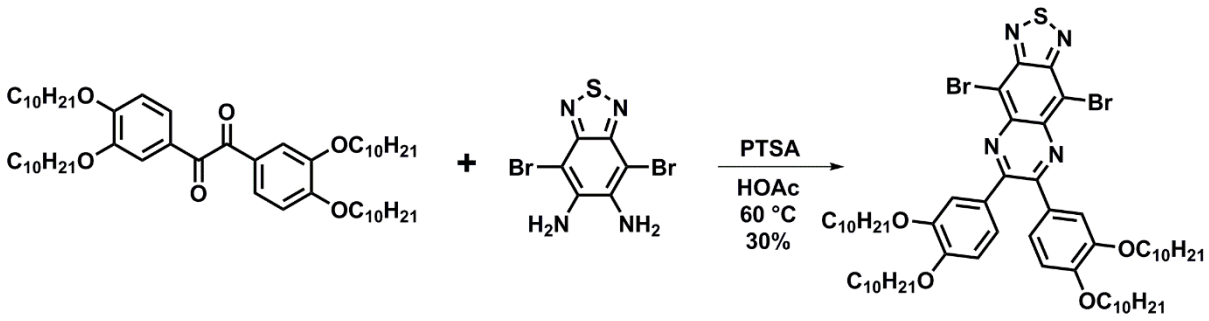

Figure 18. Synthesis of 6,7-bis(3,4-bis(decyloxy)phenyl)-4,9-dibromo-[1,2,5]thiadiazolo[3,4-g]quinoxaline

In a two necked bottom flask 1,2-bis(3,4-bis(decyloxy)phenyl)ethane-1,2-dione (0.78 g, 0.93 mmol) and 4,7-dibromobenzo[c][1,2,5]thiadiazole-5,6-diamine (0.30 g, 0.93 mmol) was dissolved with acetic acid (20 mL) under argon atmosphere. Reaction was stirred and allowed to reflux for 36 h and then the solution was poured into cold water. Precipitate was washed with cold ethanol (2x250 mL). The crude product was purified by column chromatography on silica gel using Petroleum ether/ $CHCl_3$ (1: 1) and Hexane/ DCM (1: 3) as eluent, respectively. Red solid was further purified with recrystallization method under hexane atmosphere to yield 310 mg.

^{1}H NMR (400 MHz, $CDCl_3$) δ 7.41 (d, J = 2.0 Hz, 2H), 7.34 (dd, J = 8.4, 1.9 Hz, 2H), 6.85 (d, J = 8.5 Hz, 2H), 4.04 (t, J = 6.6 Hz, 4H), 3.92 (t, J = 6.6 Hz, 4H), 1.80 (ddd, J = 28.3, 14.6, 6.9 Hz, 8H), 1.52 – 1.20 (m, 54H), 0.94 – 0.84 (m, 12H).

2.2.7 Synthesis of 3-(bromomethyl)heptane

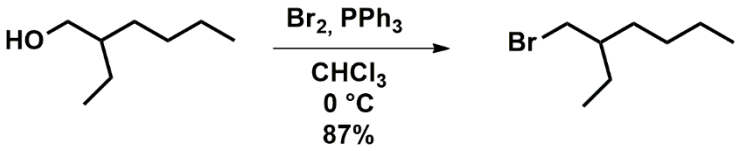

Figure 19. Synthesis of 3-(bromomethyl)heptane

3-(bromomethyl)heptane was synthesized from its alcohol derivative. 2-ethylhexanol (6.5 g, 50.0 mmol) was dissolved in 100 mL of DCM. PPh_3 (13.8 g, 52.5 mmol) was added into the solution at 0 °C under ambient atmosphere. Br_2 (18.0 g, 115 mmol) was added into the solution and stirred for half an hour at that temperature. After monitoring TLC saturated $NaHSO_3$ solution was added into mixture in order to remove excess bromine. Organic part was washed with water and dried over Na_2SO_4. After being dried in a vacuum the crude product was purified by silica gel chromatography using hexane as eluent to obtain colorless oil (8.4 g, 87% yield) [60].

^{1}H NMR (400 MHz, $CDCl_3$) δ 3.69 – 3.21 (m, 2H), 1.67 – 1.11 (m, 9H), 1.06 – 0.68 (m, 6H).

2.2.8 Synthesis of 2-(2-ethylhexyl)thiophene

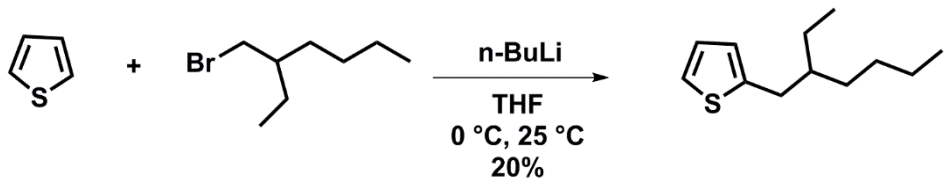

Figure 20. Synthesis of 2-(2-ethylhexyl)thiophene

Thiophene (1.44 g, 17.1 mmol) was dissolved into freshly distilled THF (10 mL) in a two-neck bottom flask protected by argon. The solution was flushed with argon for 15 min, and then the medium was cooled down to -78 °C using dry ice and acetone. 2.7 M n-butyllithium solution in toluene (7.5 mL, 20 mmol) was added dropwise by syringe over 2 h. The solution was stirred at room temperature for 2 h. After that the oil bath was warmed to 60 °C gradually and 3-(bromomethyl)heptane (3.0 g, 15.5 mmol) was added into the reaction mixture within 1 h. After the reaction was stirred overnight at 60 °C the reaction mixture was poured into cold water (250 mL) and extracted with chloroform (50 mL). Organic layer was evaporated and the residue was purified by chromatography on silica gel with heptane to give the title compound as a yellowish oil (0.60 g, 20% yield) [61].

^{1}H NMR (400 MHz, $CDCl_3$) δ 7.11 (dd, J = 5.1, 1.1 Hz, 1H), 6.92 (dd, J = 5.1, 3.4 Hz, 1H), 6.82 – 6.71 (m, 1H), 2.77 (d, J = 6.6 Hz, 2H), 1.41 – 1.21 (m, 11H), 0.89 (t, J = 7.4 Hz, 6H).

^{13}C NMR (100 MHz, $CDCl_3$) δ 144.4, 126.5, 125.0, 122.9, 41.5, 33.8, 32.4, 28.9, 25.5, 23.0, 14.1, 10.8.

2.2.9 Synthesis of 4,8-bis(5-(2-ethylhexyl)thiophen-2-yl)benzo[1,2-b:4,5-b']dithiophene

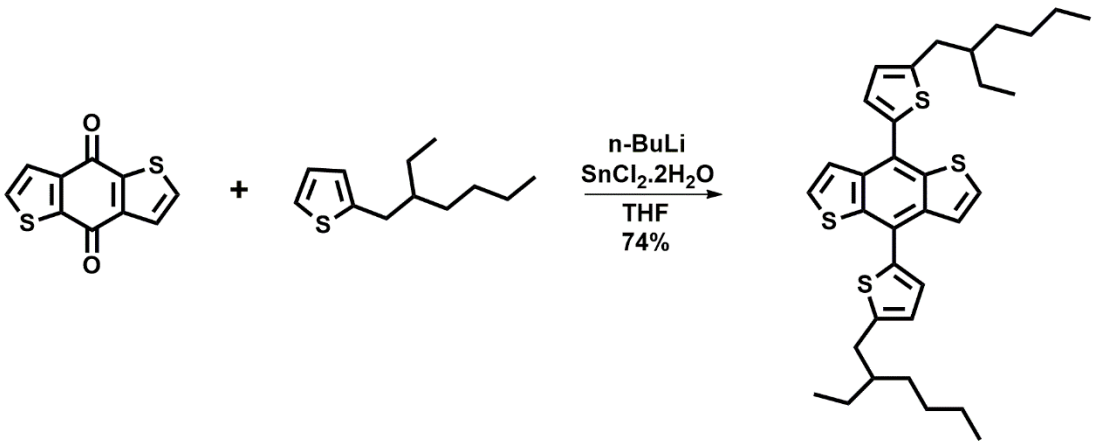

Figure 21. Synthesis of 4,8-bis(5-(2-ethylhexyl)thiophen-2-yl)benzo[1,2-b:4,5-b']dithiophene

A solution of 2-(2-ethylhexyl)thiophene (0.80 g, 4.09 mmol) in freshly distilled THF (17 mL) was cooled down to 0 °C using an ice bath. 2.7 M n-butlylithium in toluene (1.43 mL, 3.88 mmol) was added by syringe dropwise under inert atmosphere at 0 °C. The reaction mixture was heated up to 50 °C gradually and stirred at that temperature for 1 h. Subsequently, benzo[1,2-b:4,5-b']dithiophene-4,8-dione (0.30 g, 1.36 mmol) was added to the reaction mixture which was then stirred additional 2 h at 50 °C. Next, when the reaction was fixed to ambient temperature, a mixture of $SnCl_2.2H_2O$ (2.41 g, 10.70 mmol) in 10 % HCl (19 mL) was added slowly. The reaction mixture was stirred at room temperature overnight. The mixture was treated with ice cold water (50 mL) and the mixture was extracted with diethyl ether three times. The organic layer was

washed with brine, dried over Na_2SO_4 and concentrated under reduced pressure, affording a yellow-orange oil. The crude residue purified by column chromatography over silica gel with hexane as the eluent, which afforded expected product as a sticky yellow oil (0.58 g, yield 74%) [61].

^{1}H NMR (400 MHz, $CDCl_3$) δ 7.64 (d, J = 5.7 Hz, 2H), 7.45 (d, J = 5.7 Hz, 2H), 7.29 (d, J = 3.4 Hz, 2H), 6.89 (d, J = 3.4 Hz, 2H), 2.86 (d, J = 6.7 Hz, 4H), 1.67 (dd, J = 12.2, 6.0 Hz, 4H), 1.52 – 1.22 (m, 16H), 1.01 – 0.83 (m, 12H).

^{13}C NMR (100 MHz, $CDCl_3$) δ 145.7, 139.1, 137.3, 136.6, 127.8, 127.5, 125.4, 124.1, 123.5, 41.5, 34.3, 32.6, 31.7, 29.0, 25.8, 23.1, 22.8, 14.2, 11.0.

2.2.10 Synthesis of 2,6-Bis(trimethyltin)-4,8-bis(5-(2-ethylhexyl)thiophen-2-yl)benzo[1,2-b:4,5-b']dithiophene

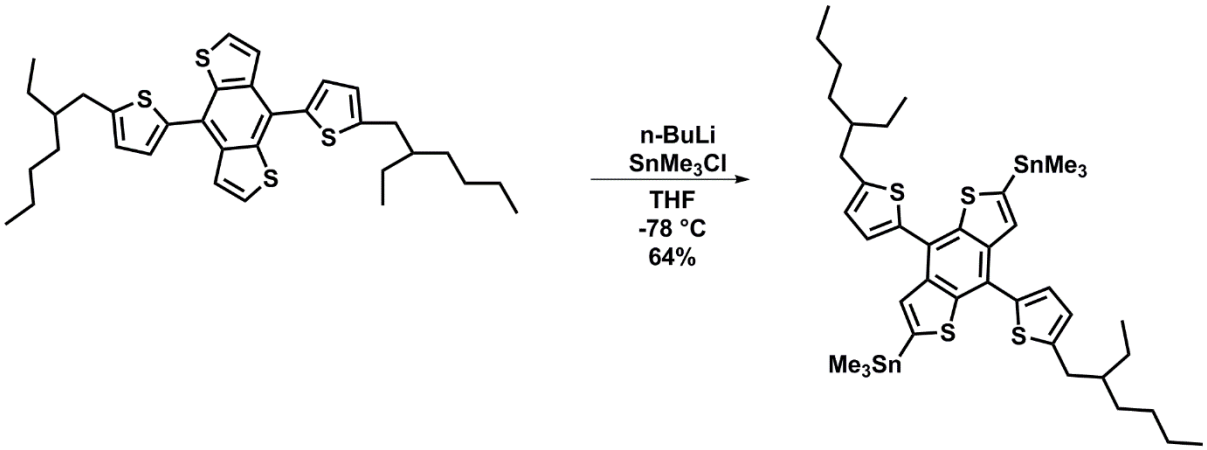

Figure 22. Synthesis of 2,6-Bis(trimethyltin)-4,8-bis(5-(2-ethylhexyl)thiophen-2-yl)benzo[1,2-b:4,5-b']dithiophene

Procedure was adapted from earlier works [61,62].

4,8-bis(5-(2-ethylhexyl)thiophen-2-yl)benzo[1,2-b:4,5-b']dithiophene (0.28 g, 0.48 mmol) was dissolved in freshly distilled THF (15 mL) under argon atmosphere. The solution was cooled down to -78 °C with dry ice and acetone. Subsequently, 2.5 M n-butyllithium in hexane (0.58 mL, 1.45 mmol) was added dropwise into the reaction

medium. The color of the solution turned to dark green just after the addition of n-butyllithium solution. The reaction mixture was stirred additional 30 min at -78 °C and later on 1.0 M chlorotrimethylstannane in THF (1.93 mL, 1.93 mmol) was injected into the reaction mixture quickly (the mixture turned cloudy orange). The reaction mixture was stirred overnight at ambient temperature and then poured into ice cold water (100 mL). The resulting mixture was extracted with ethers three times. Organic layer was washed with brine, dried over Na_2SO_4 and concentrated under reduced pressure. The orange residue was further recrystallized several times from i-PrOH and EtOH respectively to yield the title compound as a pale yellow crystalline powder (0.28 g, 64%).

^{1}H NMR (400 MHz, $CDCl_3$) δ 7.67 – 7.56 (m, 2H), 7.24 (d, J = 5.7, 3.5 Hz, 2H), 6.83 (d, J = 3.5 Hz, 2H), 2.83 – 2.74 (m, 4H), 1.61 (dd, J = 12.2, 6.1 Hz, 2H), 1.42 – 1.11 (m, 20H), 0.92 – 0.80 (m, 12H), 0.42 – 0.23 (m, 18H).

^{13}C NMR (101 MHz, $CDCl_3$) δ 145.7, 139.1, 137.3, 136.6, 127.8, 127.5, 125.4, 124.1, 123.5, 41.5, 34.3, 32.6, 29.0, 25.8, 23.1, 14.2, 11.0.

2.2.11 Synthesis of P1

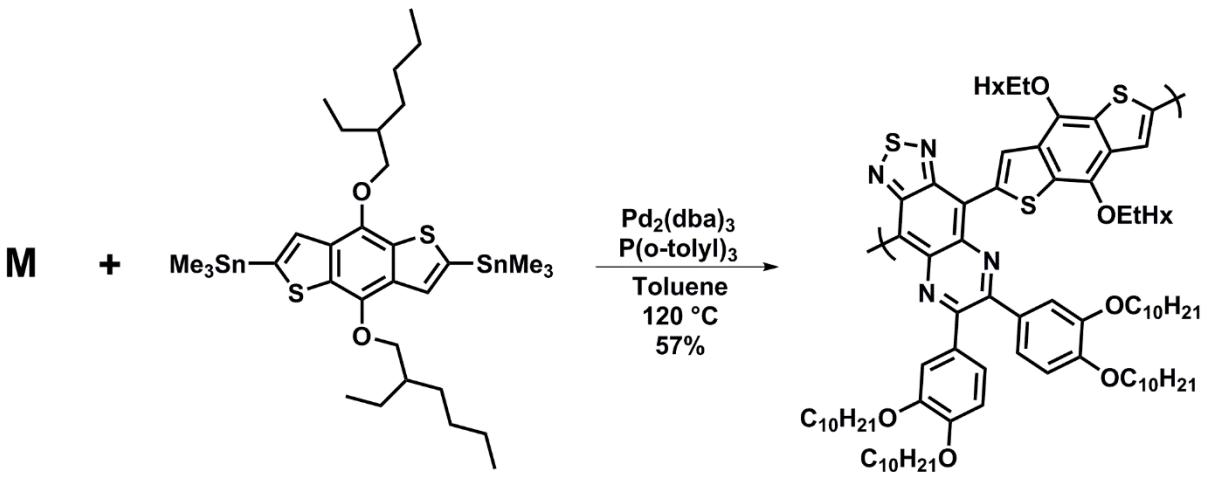

Figure 23. Synthesis of **P1**

2,6-Bis(trimethylstannyl)-4,8-bis(2-ethylhexyloxy)benzo[1,2-b:4,5-b′]dithiophene (0.13 g, 0.17 mmol) and 6,7-bis(3,4-bis(decyloxy)phenyl)-4,9-dibromo-[1,2,5]thiadiazolo[3,4-g]quinoxaline (0.19 g, 0.17 mmol) were put into schlenk tube and dried under vacuum for 1 h. After purging with argon for 30 min., 10 mL of freshly distilled toluene was added and bubbling was performed for additional 30 min in order to remove oxygen from the medium. The solution was added to two neck flask containing tris(dibenzylideneacetone)dipalladium(0) (7.72 mg, 5%) and tri(o-tolyl)phosphine (7.73 mg, 15%) under argon atmosphere. Additional bubbling was performed for 15 min and temperature was set to 120 °C. 24 h later the reaction was let to cool down to ambient temperature and then 2-bromothiophene (82.0 mg, 0.51 mmol) was added and again temperature was raised to 120 °C. 6 h later tributyl(thiophen-2-yl)stannane (0.38 g, 1.0 mmol) was introduced to reaction mixture. Polymerization was terminated by cooling down the reaction mixture to room temperature but also introducing the medium with ambient atmosphere. The crude polymer was precipitated in methanol (50 mL), filtered through a Soxhlet thimble. The n the precipitate was subjected to Soxhlet extraction with methanol, acetone, hexane and chloroform, respectively. The polymer was recovered as dark solid from chloroform fraction followed by precipitation with methanol. The solid was dried under vacuum for two days to yield **P1** (0.12 g, 57%). GPC result is as follows: number average molecular weight (M_n): 37083, molecular average molecular weight (M_w): 50976, polydispersity index (PDI): 1.37. ^{1}H NMR was shown in **Figure 52**.

2.2.12 Synthesis of P2

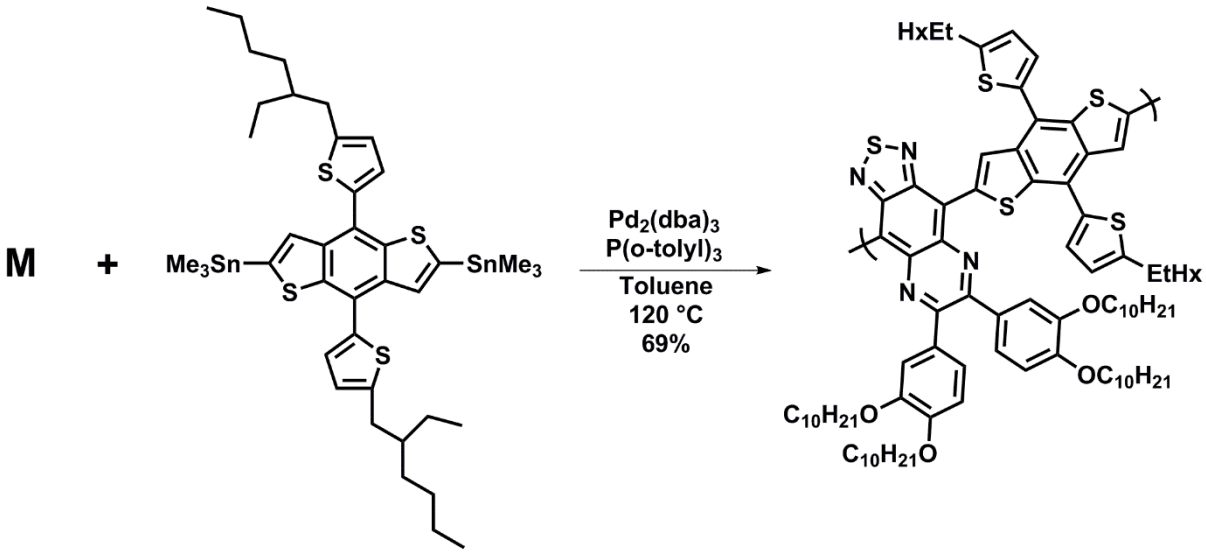

Figure 24. Synthesis of **P2**

6,7-bis(3,4-bis(decyloxy)phenyl)-4,9-dibromo-[1,2,5]thiadiazolo[3,4-g]quinoxaline (0.15 g, 0.13 mmol) and 2,6-Bis(trimethyltin)-4,8-bis(5-(2-ethylhexyl)thiophen-2-yl)benzo[1,2-b:4,5-b']dithiophene (0.12 g, 0.13 mmol) were added into flame dried two neck flask (25 mL) containing 12 mL of freshly distilled toluene. After being purged with argon for 30 min., tris(dibenzylideneacetone)dipalladium(0) (6.12 mg, 5%) and tri(o-tolyl)phosphine (6.13 mg, 15%) were added and then additional argon purge was carried out for 20 min. The reaction mixture was stirred and heated to reflux for 24 h then additional catalyst was introduced into the reaction mixture and stirred additional 16 h. Just after the addition of 2-bromothiophene (87.1 mg, 0.53 mmol) as end capper at room temperature the reaction was let to increase 120 °C. 6 h later tributyl(thiophen-2-yl)stannane (0.37 g, 1.07 mmol) was introduced to reaction mixture. Next, the mixture was cooled down to room temperature precipitated into methanol (50 mL). The crude polymer was filtered through a Soxhlet thimble and purified via Soxhlet extraction for 6 h with methanol, 6 h with acetone, 12 h with hexane and subsequently polymer was collected from chloroform. The polymer

solution was concentrated under reduced pressure and precipitated into cold methanol (50 mL). The solid was stand by under vacuum for 40 h to yield **P2** as dark solid (0.13 g, 69%). ^{1}H NMR was shown in **Figure 53**.

2.3 Conducting Polymer Characterization

2.3.1 Electrochemical Studies

Cyclic voltammetry can be used to determine the electrochemical properties of the conjugated polymer. Cyclic voltammetry (CV) is easy and efficient tool to investigate the oxidation and reduction behavior of electro-active material. Typical cyclic voltammogram was represented in **Figure 25**. The redox behavior of the conjugated polymer is monitored at a constant rate in the existence of anion of the electrolyte solution. By the determination of onset of the oxidation and reduction on the cyclic voltammogram not only HOMO and LUMO levels but also electronic band gap (Eg^{el}) can be measured. Moreover, color changes can be identified by altering the potential. In order to be able to observe the color change of the polymer, it is dissolved in chloroform and solution is sprayed onto ITO coated glass substrate. Then the coated polymer is submerged into an electrolyte- solvent couple in a UV cuvette. Moreover, Ag and Pt wire in which they behave as reference electrode and counter electrode, respectively are submerged in that cuvette.

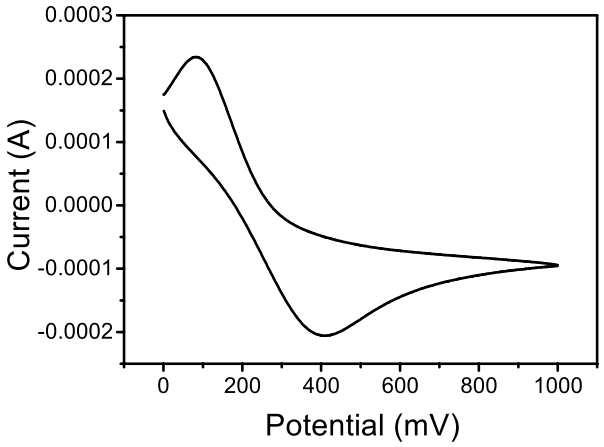

Figure 25. Representation of ferrocene in cyclic voltammogram

2.3.2 Spectroelectrochemical Studies

This technique is used to measure the absorption spectrum of the conjugated polymer at different potentials. The same three electrode system is used as mentioned above. In spectroelectrochemical analysis both neutral and doped states of the polymer are examined. Typical schematic representation of electrochemistry spectra of conjugated polymer is depicted in **Figure 26**. Also, spectroelectrochemical study helps to measure optical band gap (E^{op}) which is calculated from λ_{onset} of the polymer.

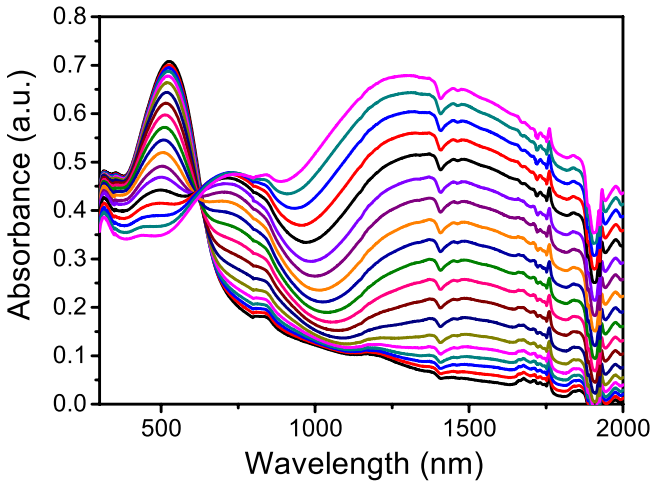

Figure 26. Schematic representation of electrochemistry of conjugated polymer

2.3.3 Kinetic Studies

Kinetic study is performed in order of determining transmittance change by altering potential continuously in between neutral and oxidized state of the polymer at the maximum absorption wavelengths as a function of time. Moreover, the time needed for a polymer to switch between reduced and oxidized states can be determined.

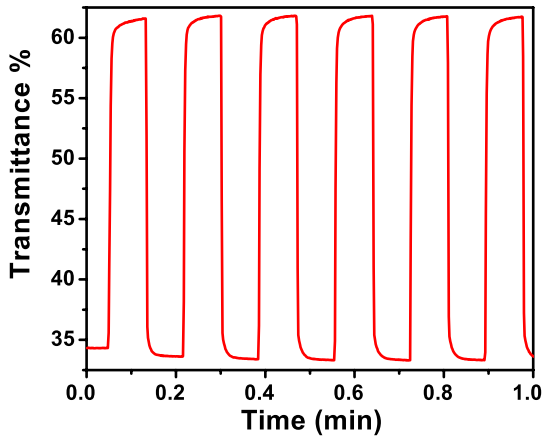

Figure 27. Representation of typical kinetic study of conjugated polymer

2.3.4 Thermal Analysis

By using thermal gravimetric analysis (TGA) degradation temperature of the conjugated polymer can be determined. The basic idea of this analysis is pointing out weight loss of the polymer with respect to increased temperature. It is said to be the point at which 5% loss in weight degradation of the polymer starts. In this analysis Perkin Elmer Pyris 1 TGA was utilized.

Similarly, in order to determine the relation between amorphous and crystalline forms of the polymers Perkin Elmer Differencial Scanning Calorimetry (DSC) was utilized. This method is used to determine glass transition temperature (T_g) and melting point (T_m) of the polymer.

2.3.5 Gel Permeation Chromatography

There are several ways to calculate average molecular weight of the synthetic polymer. In gel permeation chromatography (GPC) gel particles' pore volume plays an important role to separate polymer molecules. Physical interaction is the dominant factor in GPC analysis. Silica having a fixed pore size is used as stationary phase. Chloroform, toluene, THF are generally used for the elution of polymer solution. There is an inverse relation in between elution time and particle size or more precisely molecular weight. The basic idea is that the higher the molecular weight of the polymer smaller in retention time in GPC. Similarly, elution time increases as particle size is lowered.

2.3.6 Organic Solar Cell Applications

The fabrication of basic BHJ type organic solar cell consists of ITO/PEDOT:PSS/Polymer:PCBM/Ca:Al. The active layer (Polymer:PCBM) was prepared with different weight ratios. There are several cleaning requirements before device fabrication performance. First of all ITO was etched with a mixture of distilled water, HCl and HNO_3 at 100 °C with a ratio 50%, 49% and 1%, respectively. This process is necessary to avoid short circuit. ITO coated glass substrate was cleaned for

15 min. in an ultrasonic bath using detergent and water mixture, water, acetone and isopropyl alcohol, respectively. In order to get rid of dust particles or any other organic contaminations placed on ITO surface Harrick Plasma Cleaner was used. Subsequently, PEDOT:PSS which was filtered with 0.45μm PVDF membrane was spin coated at 5000 rpm onto ITO coated glass substrate. Then newly coated substrate was dried at 150 °C for 10 min on a hot plate. Polymer:PCBM mixture was prepared with different weight ratios in different solvents. This active layer was filtered through 0.2 μm PTFE membrane to get rid of any insoluble particles. After that filtered active layer was spin coated on PEDOT:PSS layer with various speed to get different thicknesses under nitrogen atmosphere in glove box. Then, using thermal deposition technique aluminum and calcium were deposited with 80 nm and 20 nm thickness, respectively. Current density- voltage (J-V) characteristic of the device was measured under A.M1.5 G (100 mW/cm^2).

CHAPTER 3

RESULTS AND DISCUSSION

Conjugated polymers based on D-A approach were designed and synthesized for organic solar cell applications. Thiadiazoloquinoxaline were polymerized with benzodithiophene and their electrochemical and photovoltaic properties were investigated. Two different benzodithiophene units were selected according to their strength to manipulate band gap which specifically alters optical properties and to improve photovoltaic properties in terms of V_{oc}.

3.1 Electrochemical Characterization of Polymers

3.1.1 Electrochemical Properties of Polymers

Cyclic voltammetry (CV) is carried out to determine HOMO-LUMO energy levels and redox behavior of the conjugated polymers. In order to perform cyclic voltammetry of polymers they were dissolved in chloroform (5mg/mL) and coated onto ITO substrate. As mentioned before, CV was performed in three-electrode system in 0.1 M $TBAPF_6$ (tetrabutylammonium hexafluorophosphate) and ACN solution at 100mV/s scan rate. Cyclic voltammograms of **P1** and **P2** were depicted in **Figure 28** and **Figure 29**. Electrochemical properties of polymers were summarized in **Table 1**.

Moreover, cyclic voltammograms reveal that **P1** and **P2** have only p type doping/ dedoping property. In p- type doping and dedoping processes **P1** revealed a reversible redox couple at 0.82 V and 0.40 V, respectively. Similarly, **P2** oxidized at 0.90 V and reduced at 0.63 V reversibly. Furthermore, the onset of oxidation potential of **P1** and **P2** were observed at 0.40 eV and 0.60 eV, respectively. After the determination of onset of oxidation potential, HOMO energy level of **P1** was calculated as -5.15 eV using the equation HOMO= -(4.75 eV + E_{onset}^{ox}). In the same manner **P2** was found as -5.35 eV. Due to the lack of n- type doping and dedoping property of **P1** and **P2** relative LUMO energy level of the polymers were calculated using optical band gap and HOMO energy level which had determined from CV. LUMO energy level of **P1** and **P2** were found as -4.11 eV and -4.25 eV, respectively.

It is a trivial fact that the amount of harvested photons increases as band gap decrease. As indicated in **Table 1** optical band gap was found as 1.04 eV and 1.10 eV for **P1** and **P2**, respectively. When **Table 1** was interpreted it can be said that using alkylthiophene substituted BDT moiety which was used in **P2** increased not only the magnitude of HOMO energy level but also the magnitude of LUMO. Low lying LUMO generally results with low band gap in polymer. Low lying LUMO is efficient in order to get effective intermolecular charge transfer process in between polymer and $PC_{71}BM$. When the device fabrication was considered the difference in LUMO energy level of the polymer and $PC_{71}BM$ should be in the range of 0.3-0.5 eV for effective intermolecular charge transfer. Herein, it is important to note that LUMO energy level of $PC_{71}BM$ is -3.90 eV at ambient temperature [63,64]. By looking HOMO energy levels of polymers it can be said that down- shifted HOMO energy level of **P2** results with higher V_{oc}. In the light of the findings above both **P1** and **P2** should reveal good intermolecular charge transfer process in photovoltaic applications. More down-shifted HOMO energy level of **P2** results with higher band gap [65,66].

Table 1. Summary of electrochemical and spectroelectrochemical properties of **P1** and **P2**

	$E_{p\text{-doping}}$ (V)	$E_{p\text{-dedoping}}$ (V)	HOMO (eV)	LUMO* (eV)	λmax (nm)	E_g^{op} (eV)
P1	0.82	0.40	-5.15	-4.11	400/975	1.04
P2	0.90	0.63	-5.35	-4.25	413/964	1.10

*LUMO energy level was calculated from optical band gap.

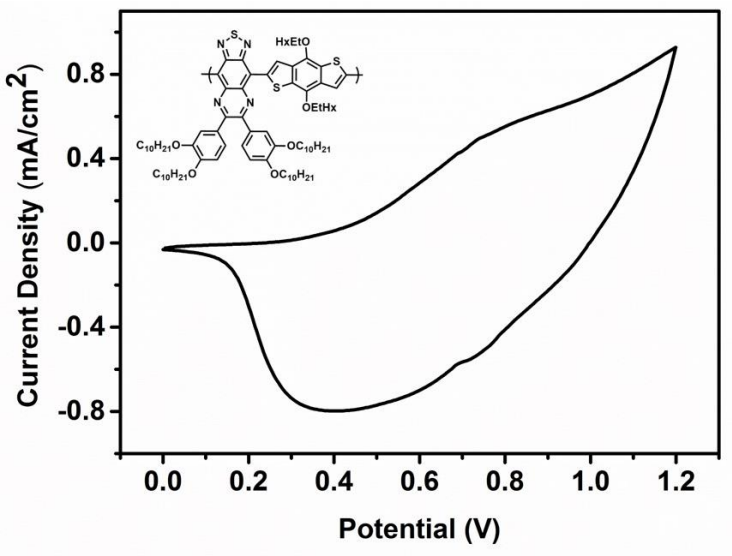

Figure 28. Cyclic voltammogram of **P1** with a scan rate of 100 mV/s

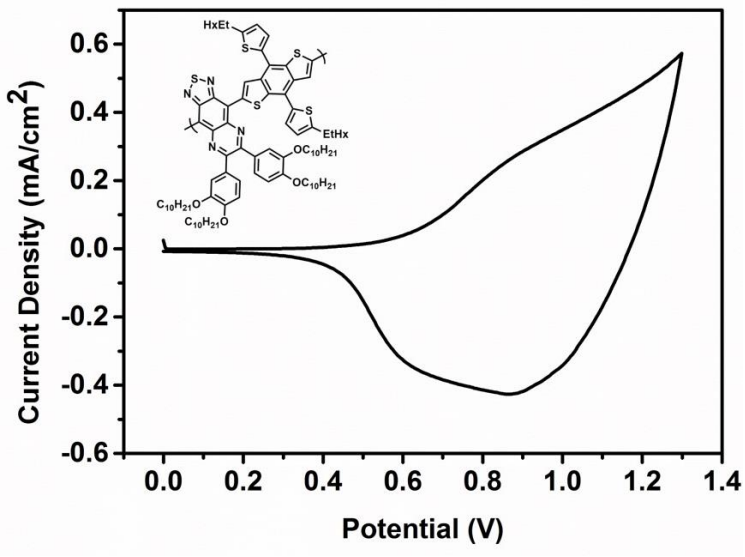

Figure 29. Cyclic voltammogram of **P2** with a scan rate of 100 mV/s

3.1.2 Scan Rate Studies of Polymers

The current density of the polymers was investigated at different scan rates in 0- 1.2 V potential interval. The change in peak current of conjugated polymers was monitored by Randles- Sevcik equation.

$$i_p = kAD^{1/2}n^{3/2}Cv^{1/2}$$

When the equation is interpreted it can be said that if there is a linear relationship between current change and scan rate electrochemical process is non-diffusion controlled and reversible. In other words, anion layer is constructed on oxidized polymer and reversible mass transfer takes place. Cyclic voltammograms of polymers at different scan rates were shown in **Figure 30** and **Figure 31**.

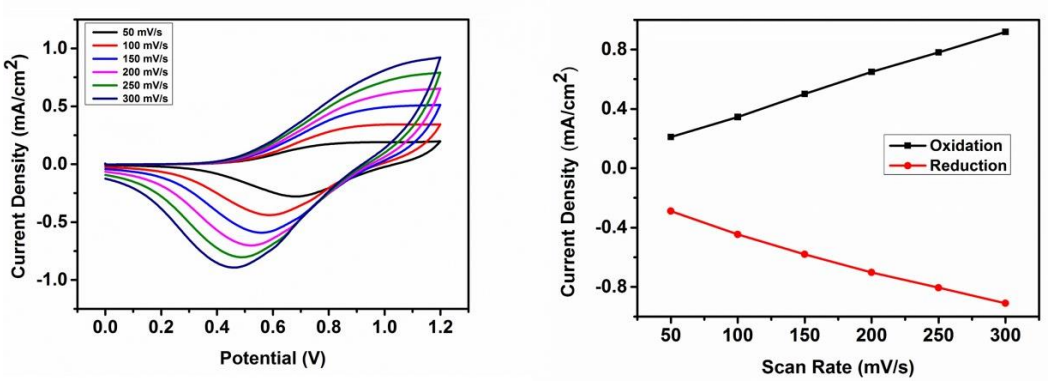

Figure 30. Cyclic voltammogram of **P1** in 0.1 M $TBAPF_6$/ACN at 50-300 mV/s scan rate interval

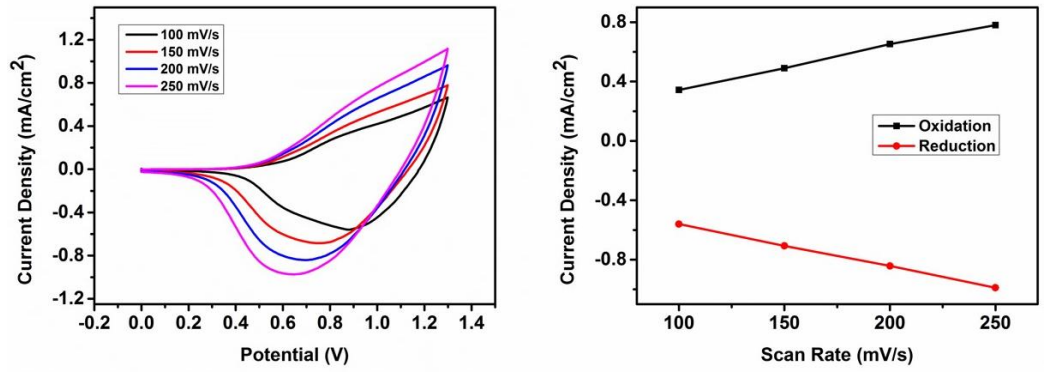

Figure 31. Cyclic voltammogram of **P2** in 0.1 M $TBAPF_6$/ACN at 50-250 mV/s scan rate interval

3.1.3 Spectroelectrochemical Properties of Polymers

In order to get quantitative information on polymers' light absorption property as a function of wavelength spectroelectrochemical studies were carried out. Polymers were dissolved in chloroform and spray coated onto ITO substrate. Absorption spectrum of the polymers were monitored in UV-Vis-NIR region for **P1** and **P2** represented in **Figure 32** and **Figure 33**, respectively.

It is important to note that the maximum absorbance seen firstly in visible region corresponds to π-π^* transition between HOMO and LUMO energy levels of the

polymers. Upon applied potential new bands so called polaron and bipolaron are formed in the spectra. The polaron was seen in visible region and bipolaron bands appeared in near infrared (NIR) region. As the potential applied onto polymer increases polymer's absorbance decreases in neutral state. On the other hand, polaron and bipolaron band intensity increase. By using three variables; Luminance (L), hue (a) and saturation (b) color of the polymers were monitored in each state. **P1** is oily yellow (L: 48, a: -3, b: 48) in its neutral state and upon oxidation of **P1** color turns to light grey (L: 31, a: -3, b: -2). When the color of the polymers was considered there is a slight difference in between **P1** and **P2**. **P2** is oily yellow in its neutral state (L: 43, a: -7, b: 44) and color shifts to grey (L: 43, a: -2, b: 6) in its oxidized state. L a b values of the polymers were summarized in **Table 2**.

Table 2. Summary of L a b values of the polymers

L a b values				
P1	0.0 V	0.9 V	1.1 V	1.2 V
	48	38	36	31
	-3	0	-1	-3
	48	16	3	-2
P2	0.0 V	0.9 V	1.1 V	1.2 V
	43	49	46	43
	-7	-3	-1	-2
	44	22	9	6

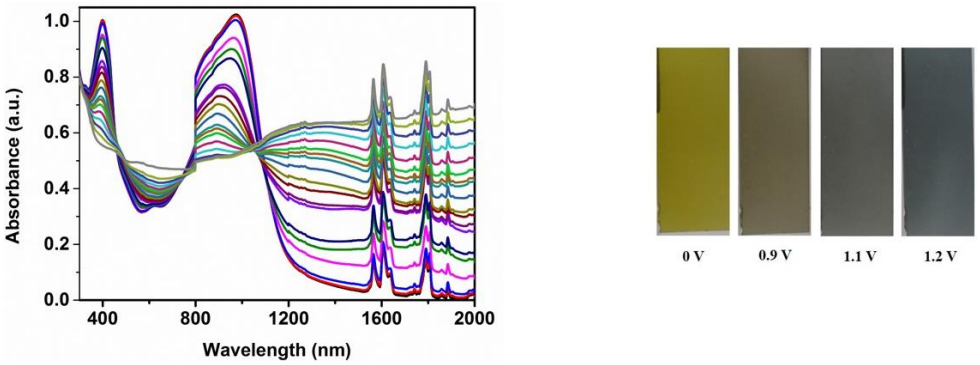

Figure 32. UV-Vis-NIR spectra and colors of **P1**

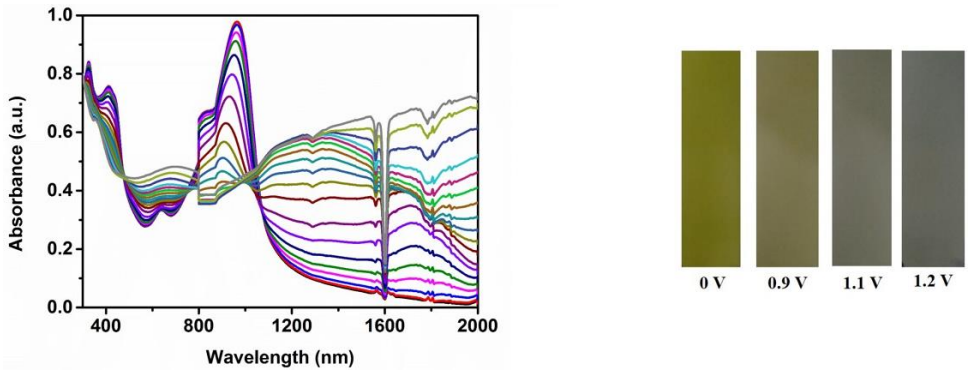

Figure 33. UV-Vis-NIR spectra and colors of **P2**

3.1.4 Kinetic Studies of P1 and P2

In addition to electrochemical and spectroelectrochemical properties kinetic studies also plays an important role in electronic device applications. In kinetic studies switching time and percent transmittance properties were followed. In order to calculate switching time and percent transmittance potential was applied in between neutral and oxidized state of the polymers with 5 s time interval. Polymers' switching time and optical contrast behaviors are summarized in **Table 2**. Optical contrast values were determined at which polymers reveal maximum absorbance in the spectrum. When the results were interpreted it can be said that there is a slight optical contrast difference in between **P1** and **P2**. **P1** revealed 87%, 19% and 22% optical contrast at 1940, 975 and 400 nm, respectively. Besides that, its thiophene based counterpart

revealed poor optical contrast in visible region compared to **P1** as 7% optical contrast at 425 nm. Optical contrasts of **P2** was obtained as 20% at 960 nm and 87% at 1880 nm. It can be said that both **P1** and **P2** unfortunately cannot be used in visible region for electronic device applications. On the other hand, 87% optical contrast result at around 1900 nm for **P1** and **P2** is very promising to be employed in NIR region.

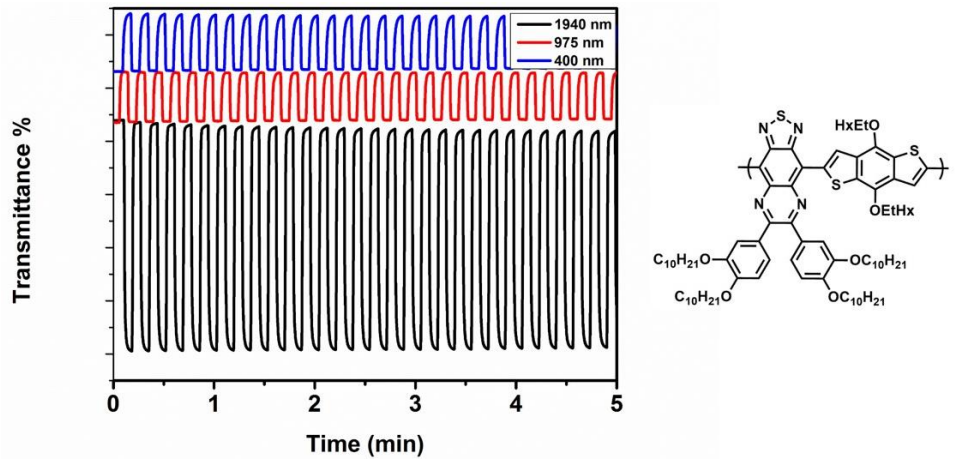

Figure 34. Percent transmittance change and switching times of **P1** at its maximum wavelengths

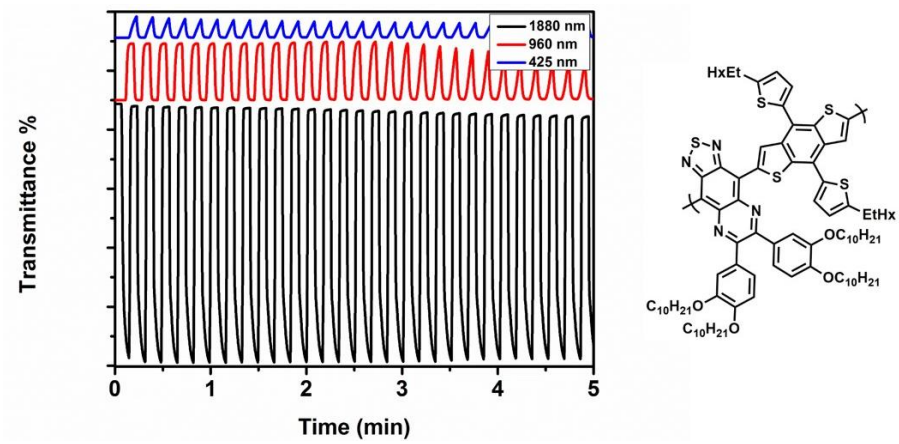

Figure 35. Percent transmittance change and switching times of **P1** at its maximum wavelengths

Table 3. Switching times and optical contrast of **P1** and **P2**

	Optical contrast (ΔT %)		Switching times (s)
P1	87	1940 nm	1.2
	19	975 nm	0.9
	22	400 nm	1.2
P2	87	1880 nm	1.3
	20	960 nm	1.4
	7	425 nm	1.0

Surprisingly, the switching times of the polymers exhibit interesting results. **P1** having alkoxy group in BDT unit has 1.2, 0.9 and 1.2 s switching times at its maximum wavelengths as 1940 nm, 975 nm and 400 nm, respectively. Similarly, switching times of **P2** are 1.3 s, 1.4 s and 1.0 s at 1880 nm, 960 nm and 425 nm respectively. Even if the results are quite close to each other theoretically **P2** should reveal lower switching time due to its alkylated thiophene unit on the polymer backbone. As indicated previously, 2-D configuration of BDT unit ease doping/de-doping mechanism. On the other hand, in this case it is just the opposite in NIR region. This can be explained by 2-D conjugated BDT unit which has two maximum wavelength in the spectrum [46].

3.1.5 Thermal Analysis

Using thermogravimetry analyses (TGA) thermal behaviors of the polymers were investigated under protected N_2 atmosphere with a heating rate of 10 °C/ min. 5% weight loss was observed at 325 °C and 440 °C for **P1** and **P2**, respectively. TGA and DSC analysis of **P1** and **P2** were depicted in Appendices part (**Figure 58-61**).

3.2 Photovoltaic Studies

Chemically synthesized polymers were used as donor material and $PC_{71}BM$ was used as acceptor in bulk heterojunction solar cell device. In order to overcome the solubility problem of thiadiazoloquinoxaline moiety two different alkyl chains were used.

The current density versus voltage curves of **P1**:$PC_{71}BM$ and **P2**:$PC_{71}BM$ in bulk heterojunction solar cell were depicted in **Figure 36** and **Figure 37**. Power conversion efficiencies of synthesized polymers are determined at different weight ratios. The results of the devices were collected in **Table 3** and **Table 4**. The highest power conversion efficiency was reported as 0.73% in (**P2**:$PC_{71}BM$) 1:2 weight ratio after the optimization was done with 1 vol. % with diiodooctane (DIO) for **P2**. From these results it can be said that the photovoltaic performance of **P2** based devices can be improved by introducing additive to the device construction which was shown in **Figure 38**. With this optimization V_{oc} of **P2** based device was enhanced slightly. Even if the FF value decreased after the optimization studies PCE increased due to the increase in J_{sc}. The highest PCE was monitored as 0.33 % for **P1**. The reason of low PCE of **P1** based device mainly arises from very low V_{oc} value (0.38 mA/cm^2). Also, the reason of being low V_{oc} value is most probably the mismatch of the absorption of the polymer.

When the performance of the devices prepared with **P1** and **P2** is compared, there is a slight difference in their V_{oc} values. As already pointed out by L. Hou et al., 2-D conjugated BDT units are superior due to its coplanar structure which eases the charge transfer compared to its alkoxy or alkylated derivatives [45]. This could be the one of the possible reasons of lower V_{oc} value of **P1**. In addition, since the alkoxy has strong electron donating effect, high lying HOMO level was recorded for **P1** (-5.15 eV) compared to that of **P2** (-5.35 eV). Because of these two effect which is related with the alkoxy group in the polymer backbone, V_{oc} of the **P1** based solar cell was lower. Overall, it can be said that low PCE of the polymers is most probably the mismatch of LUMO energy level of the polymers and LUMO energy level of $PC_{71}BM$.

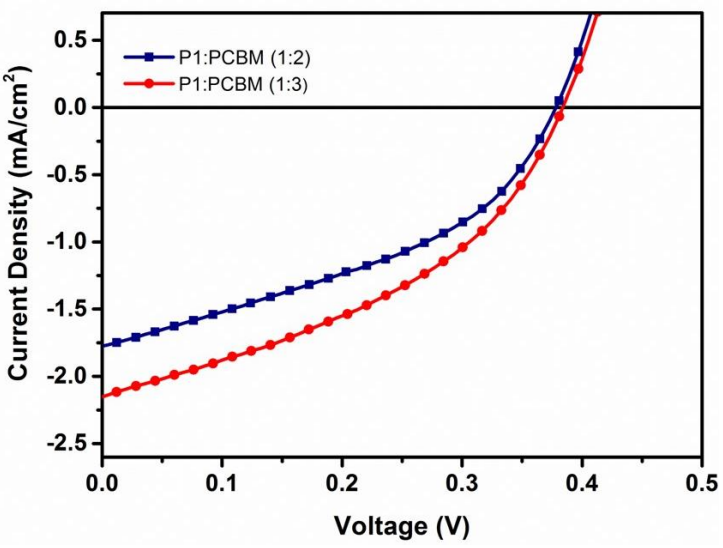

Figure 36. Current- voltage characteristic of **P1**

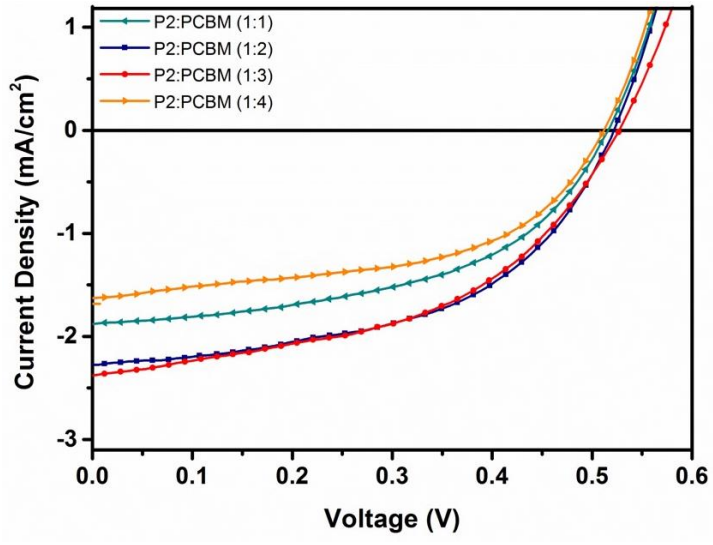

Figure 37. Current- voltage characteristic of **P2**

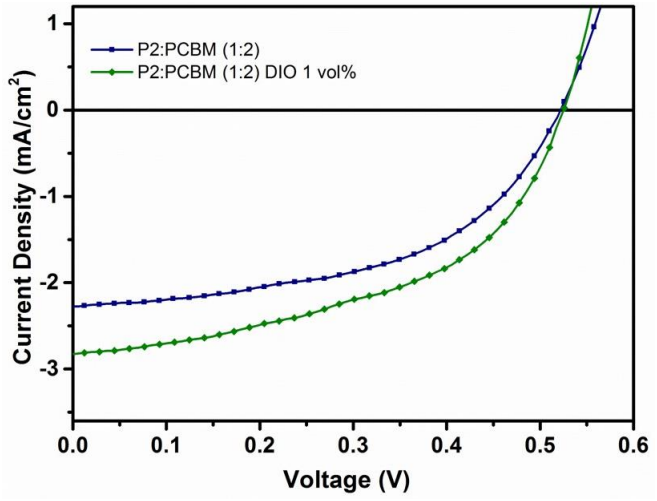

Figure 38. Current density- voltage characteristic of **P2** when DIO is used as additive

Table 4. Summary of photovoltaic studies of **P1**

P1:PCBM	V_{oc} (V)	J_{sc} (mA/cm^2)	V_{max} (V)	J_{max} (mA/cm^2)	FF (%)	PCE (%)
1:2	0.38	1.77	0.26	1.04	40	0.27
1:3	0.38	2.16	0.26	1.28	40	0.33

Table 5. Summary of photovoltaic studies of **P2**

P2:PCBM	V_{oc} (V)	J_{sc} (mA/cm^2)	V_{max} (V)	J_{max} (mA/cm^2)	FF (%)	PCE (%)	
1:1	0.52	1.87	0.36	1.38	51	0.49	
1:2	0.52	2.28	0.37	1.63	51	0.60	
1:3	0.53	2.39	0.36	1.64	47	0.59	
1:4	0.51	1.64	0.38	1.14	52	0.43	
1:1	0.52	2.82	0.40	1.83	50	0.73	1 vol % DIO

CHAPTER 4

CONCLUSION

In this study two D-A type conjugated polymers were chemically synthesized via Stille coupling reaction for photovoltaic applications.

In order to investigate the effect of donor moiety on the polymer backbone two different BDT containing donor units were used. **P1** containing alkoxy group substituted in 4- and 8- positions of BDT unit showed lower band gap due to its electron donating effect of alkoxy group. Kinetic studies showed that both **P1** and **P2** have switching times in the range of 0.9 to 1.4 s. In addition to switching times, polymers exhibited high stability in NIR region with high optical contrast as 87%. Optical and electrochemical studies showed that polymers have low band gap at around 1.0 eV.

Using bulk heterojunction system power conversion efficiency of the polymers were monitored. The highest PCE of 0.73 % was found in the case of **P2** based devices with V_{oc}, J_{sc} and FF values of 0.52 V, 2.82 mA/cm^2 and 0.50 % respectively. Higher device performance of the **P2** with respect to **P1** is the resulted from the contribution of the alkylthiophene substitution in **P2** backbone. Therefore, structural modification done by substitution of different groups onto BDT seems a reasonable way to manipulate photovoltaic properties of the polymers.

REFERENCES

[1] C.K. Chiang, C.R. Fincher, Y.W. Park, A.J. Heeger, H. Shirakawa, E.J. Louis, S.C. Gau, A.G. MacDiarmid, Phys. Rev. Lett. 39 (1977) 1098–1101.

[2] N. Co-investigator, J. Chem. Inf. Model. 53 (2013) 1689–1699.

[3] J. Roncali, Chem. Rev. 92 (1992) 711–738.

[4] J. Roncali, J. Mater. Chem. 9 (1999) 1875–1893.

[5] M. Wan, Conducting Polymers with Micro or Nanometer Structure, 2008.

[6] Y. Cheng, S. Yang, C. Hsu, Chem. Rev. 109 (2009) 5868–5923.

[7] A.G. MacDiarmid, A.J. Epstein, Synth. Met. 69 (1995) 85–92.

[8] S. Gunes, H. Neugebauer, N.S. Sariciftci, Chem. Rev. 107 (2007) 1324–1338.

[9] C.J. Brabec, A. Cravino, D. Meissner, N.S. Sariciftci, T. Fromherz, M.T. Rispens, L. Sanchez, J.C. Hummelen, Adv. Funct. Mater. 11 (2001) 374–380.

[10] M.C. Scharber, N.S. Sariciftci, Prog. Polym. Sci. 38 (2013) 1929–1940.

[11] B. Kadem, A. Hassan, W. Cranton, J. Mater. Sci. Mater. Electron. 27 (2016) 1–11.

[12] Y. Li, Acc. Chem. Res. 45 (2012) 723–733.

[13] J. Roncali, Macromol. Rapid Commun. 28 (2007) 1761–1775.

[14] H.A.M. van Mullekom, J. Vekemans, E.W. Meijer, Chem. Eur. J. 4 (1998) 1235–1243.

[15] C. Winder, N.S. Sariciftci, J. Mater. Chem. 14 (2004) 1077.

[16] J.Y. Lee, S.W. Heo, H. Choi, Y.J. Kwon, J.R. Haw, D.K. Moon, Sol. Energy Mater. Sol. Cells 93 (2009) 1932–1938.

[17] D. Wöhrle, D. Meissner, Adv. Mater. 3 (1991) 129–138.

[18] M.S.A. Abdou, L. Xiaotang, W. Zi, F. Orfino, M.J. Deen, S. Holdcroft, Chem. Mater. 7 (1995) 631–641.

[19] R.D. McCullough, Adv. Mater. 10 (1998) 93–116.

[20] N.S. Sariciftci, D. Braun, C. Zhang, V.I. Srdanov, A.J. Heeger, G. Stucky, F. Wudl, Appl. Phys. Lett. 62 (1993) 585.

[21] C.W. Tang, Appl. Phys. Lett. 48 (1986) 183.

[22] F.C. Krebs, Sol. Energy Mater. Sol. Cells 93 (2009) 394–412.

[23] A. Facchetti, Chem. Mater. 23 (2011) 733–758.

[24] G. Yu, J. Gao, J.C. Hummelen, F. Wudl, A.J. Heeger, Science 270 (1995) 1789–1791.

[25] H. Antonio, S. Hegedus, Handbook of Photovoltaic Science and Engineering, 2003.

[26] A. Singh, S.K. Gupta, A. Garg, Org. Electron. 35 (2016) 118–127.

[27] T. Xu, L. Yu, Mater. Today 17 (2014) 11–15.

[28] Z. Zhang, J. Wang, J. Mater. Chem. 22 (2012) 4178.

[29] T. Fromherz, F. Padinger, D. Gebeyehu, C. Brabec, J.C. Hummelen, N.S. Sariciftci, Sol. Energy Mater. Sol. Cells 63 (2000) 61–68.

[30] B.R. Saunders, J. Colloid Interface Sci. 369 (2012) 1–15.

[31] A. Liscio, G. De Luca, F. Nolde, V. Palermo, K. Müllen, P. Samorì, J. Am. Chem. Soc. 130 (2008) 780–781.

[32] G.P. Smestad, Sol. Energy Mater. Sol. Cells 55 (1998) 157–178.

[33] L. Yang, L. Yan, W. You, J. Phys. Chem. Lett. 4 (2013) 1802–1810.

[34] C. Kitamura, S. Tanaka, Y. Yamashita, Chem. Mater. 8 (1996) 570–578.

[35] Y. Lee, Y.M. Nam, W.H. Jo, J. Mater. Chem. 21 (2011) 8583–8590.

[36] R. Duan, L. Ye, X. Guo, Y. Huang, P. Wang, S. Zhang, J. Zhang, L. Huo, J. Hou, Macromolecules 45 (2012) 3032–3038.

[37] C. Bathula, C.E. Song, W.H. Lee, J. Lee, S. Badgujar, R. Koti, I.N. Kang, W.S. Shin, T. Ahn, J.C. Lee, S.J. Moon, S.K. Lee, Thin Solid Films 537 (2013) 231–238.

[38] J.Y. Lee, W.S. Shin, J.R. Haw, D.K. Moon, J. Mater. Chem. 19 (2009) 4938–4945.

[39] H. Qin, L. Li, T. Liang, X. Peng, J. Peng, Y. Cao, J. Polym. Sci. Part A Polym. Chem. 51 (2013) 1565–1572.

[40] M.Y. Sen, J.E. Puskas, Am. Chem. Soc. Polym. Prepr. Div. Polym. Chem. 49 (2008) 487–488.

[41] T.L.D. Tam, T. Salim, H. Li, F. Zhou, S.G. Mhaisalkar, H. Su, Y.M. Lam, A.C. Grimsdale, J. Mater. Chem. 22 (2012) 18528–18534.

[42] Y. Lee, T.P. Russell, W.H. Jo, Org. Electron. Physics, Mater. Appl. 11 (2010) 846–853.

[43] H.-Y. Chuang, S.-C. Hsu, P.-I. Lee, J.-F. Lee, S.-Y. Huang, S.-W. Lin, P.-Y. Lin, Polym. Bull. 71 (2014) 1117–1130.

[44] Y. Hou, J., Chen, H.-Y., Zhang, S., Yang, J. Phys. Chem. C 113 (2009) 21202–21207.

[45] L. Huo, J. Hou, Polym. Chem. 2 (2011) 2453.

[46] Y.S. Byun, J.H. Kim, J.B. Park, I.N. Kang, S.H. Jin, D.H. Hwang, Synth. Met. 168 (2013) 23–30.

[47] M.L. Keshtov, D. V Marochkin, V.S. Kochurov, A.R. Khokhlov, E.N.

Koukaras, G.D. Sharma, J. Mater. Chem. A 2 (2014) 155–171.

[48] S. Wen, X. Bao, W. Shen, C. Gu, Z. Du, L. Han, D. Zhu, R. Yang, J. Polym. Sci. Part A Polym. Chem. 52 (2014) 208–215.

[49] T. Bilkay, K. Schulze, T. Egorov-Brening, K. Fink, S. Janietz, Org. Electron. 14 (2013) 344–353.

[50] P. Sista, H. Nguyen, J.W. Murphy, J. Hao, D.K. Dei, K. Palaniappan, J. Servello, R.S. Kularatne, B.E. Gnade, B. Xue, P.C. Dastoor, M.C. Biewer, M.C. Stefan, Macromolecules 43 (2010) 8063–8070.

[51] J.Y. Zhou, Y. Zuo, X.J. Wan, G.K. Long, Q. Zhang, W. Ni, Y.S. Liu, Z. Li, G.R. He, C.X. Li, B. Kan, M.M. Li, Y.S. Chen, J. Am. Chem. Soc. 135 (2013) 8484–8487.

[52] Y. Chen, Y. Yan, Z. Du, X. Bao, Q. Liu, V. a. L. Roy, M. Sun, R. Yang, C.S. Lee, J. Mater. Chem. C 2 (2014) 3921.

[53] D. Gedefaw, M. Tessarolo, W. Zhuang, R. Kroon, E. Wang, M. Bolognesi, M. Seri, M. Muccini, M.R. Andersson, Polym. Chem. 5 (2014) 2083.

[54] H. Zhou, L. Yang, A.C. Stuart, S.C. Price, S. Liu, W. You, Angew. Chemie - Int. Ed. 50 (2011) 2995–2998.

[55] A. Balan, D. Baran, G. Gunbas, A. Durmus, F. Ozyurt, L. Toppare, Chem. Commun. (Camb). 60 (2009) 6768–6770.

[56] F. Zhang, O. Inganäs, M.R. Andersson, Org. Lett. 12 (2010) 4470–4473.

[57] X.X. Sun, X.X. Zhuang, Y.L. Ren, Adv. Mater. Res. 482–484 (2012) 1221–1224.

[58] T.T. Steckler, P. Henriksson, S. Mollinger, A. Lundin, A. Salleo, M.R. Andersson, J. Am. Chem. Soc. 136 (2014) 1190–1193.

[59] S. Kato, N. Takahashi, H. Tanaka, A. Kobayashi, T. Yoshihara, S. Tobita, T.

Yamanobe, H. Uehara, Y. Nakamura, Chem. - A Eur. J. 19 (2013) 12138–12151.

[60] F. He, W. Wang, W. Chen, T. Xu, S.B. Darling, J. Strzalka, Y. Liu, L. Yu, J. Am. Chem. Soc. 133 (2011) 3284–3287.

[61] L. Huo, S. Zhang, X. Guo, F. Xu, Y. Li, J. Hou, Angew. Chemie - Int. Ed. 50 (2011) 9697–9702.

[62] H.-S. Chung, W.-H. Lee, C.E. Song, Y. Shin, J. Kim, S.K. Lee, W.S. Shin, S.-J. Moon, I.-N. Kang, Macromolecules 47 (2014) 97–105.

[63] S. Yoo, J. Kum, S. Cho, Nanoscale Res. Lett. 6 (2011) 545.

[64] H. Derouiche, S. Saidi, A.B. Mohamed, Smart Grid Renew. Energy 2 (2011) 278–281.

[65] V. Tamilavan, M. Song, S.-H. Jin, M.H. Hyun, Macromol. Res. 21 (2013) 406–413.

[66] G. Li, R. Zhu, Y. Yang, Nat. Photonics 6 (2012) 153–161.

APPENDICES

NMR DATA

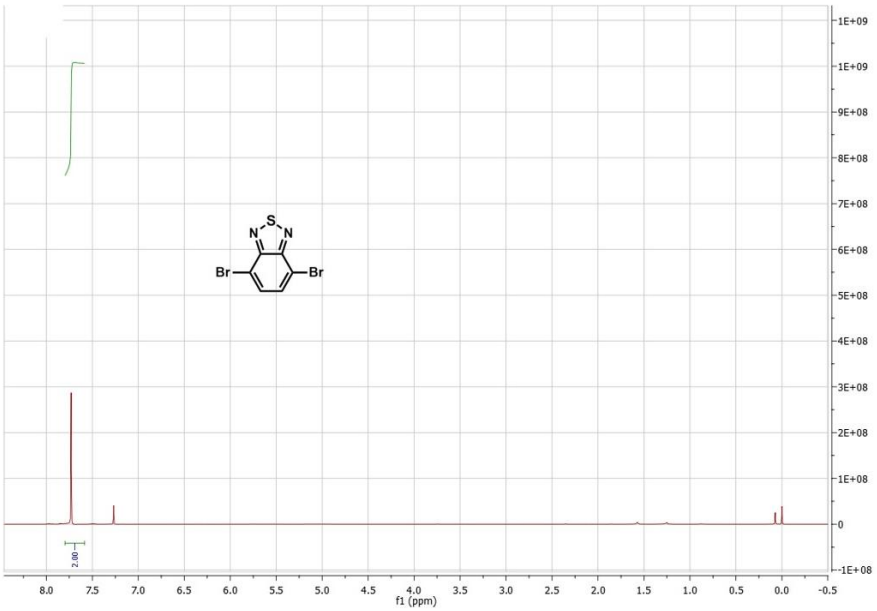

Figure 39. ^{1}H NMR result of 4,7-dibromobenzo[c][1,2,5]thiadiazole

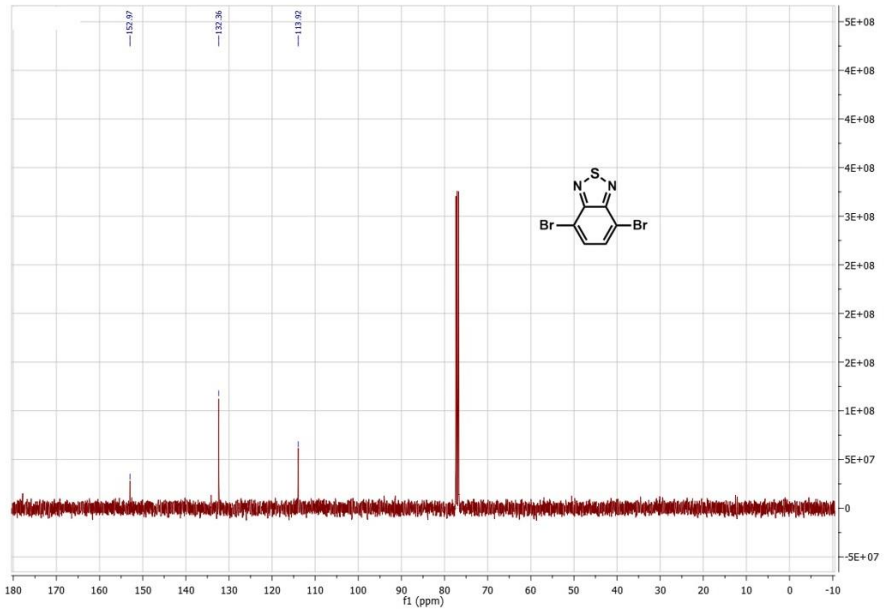

Figure 40. ^{13}C NMR result of 4,7-dibromobenzo[c][1,2,5]thiadiazole

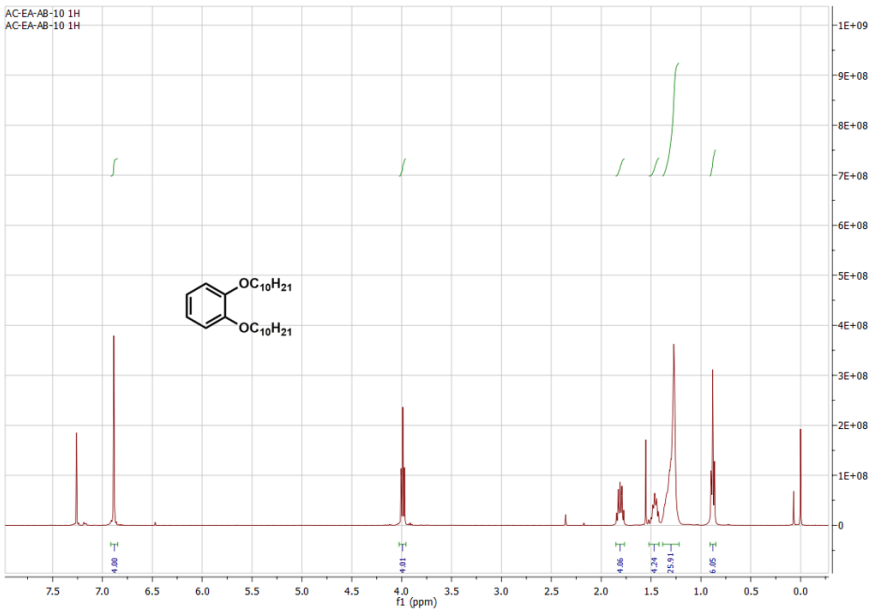

Figure 41. [1]H NMR result of 1,2-bis(decyloxy)benzene

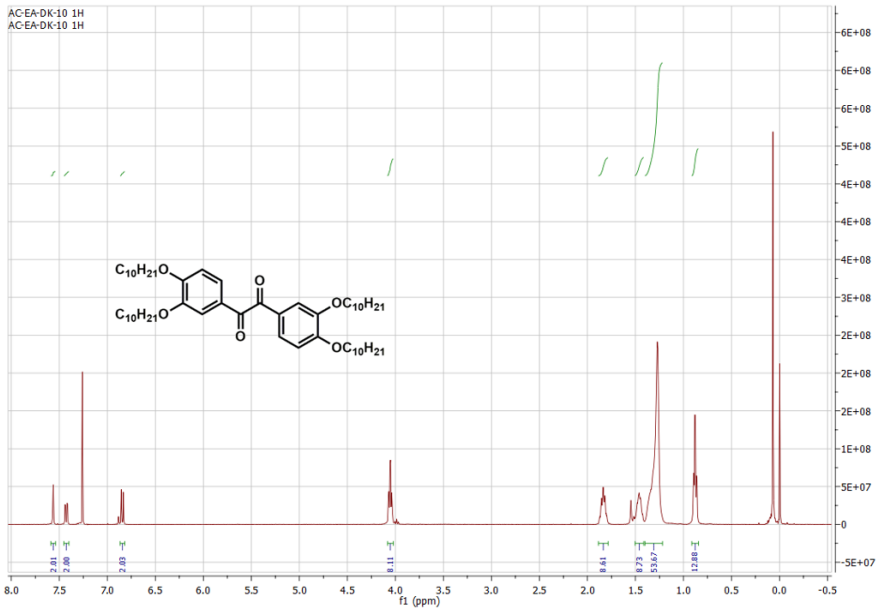

Figure 42. [1]H NMR result of 1,2-bis(3,4-bis(decyloxy)phenyl)ethane-1,2-dione

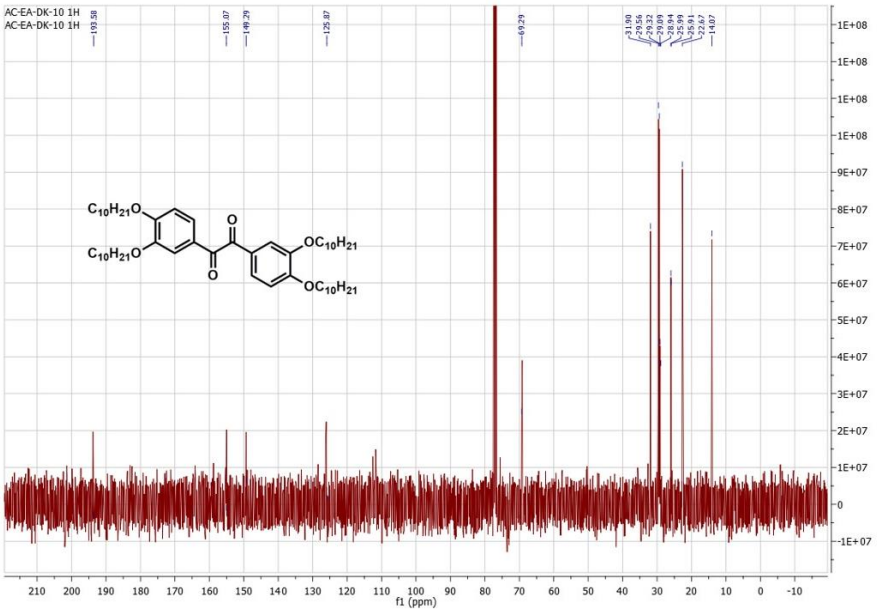

Figure 43. ^{13}C NMR result of 1,2-bis(3,4-bis(decyloxy)phenyl)ethane-1,2-dione

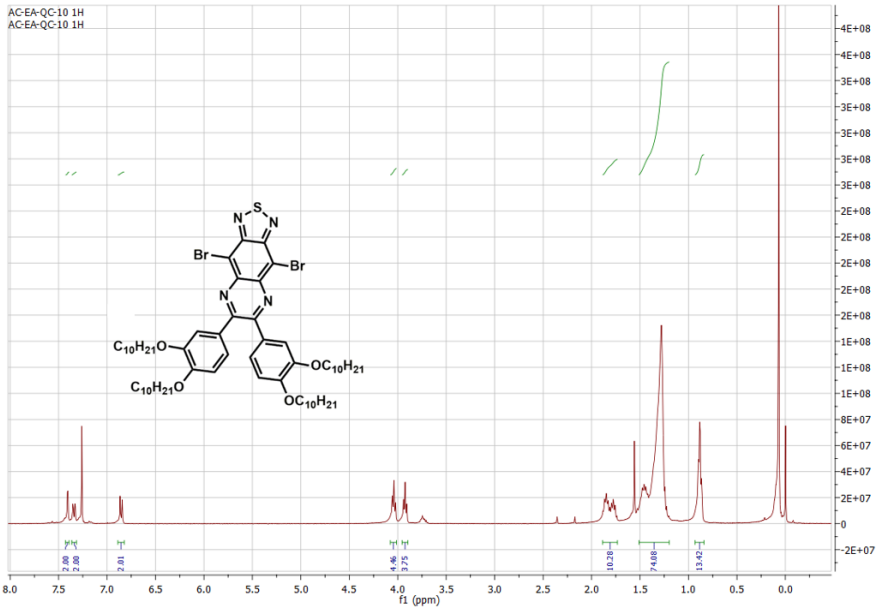

Figure 44. ^{1}H NMR result of 6,7-bis(3,4-bis(decyloxy)phenyl)-4,9-dibromo-[1,2,5]thiadiazolo[3,4-g]quinoxaline

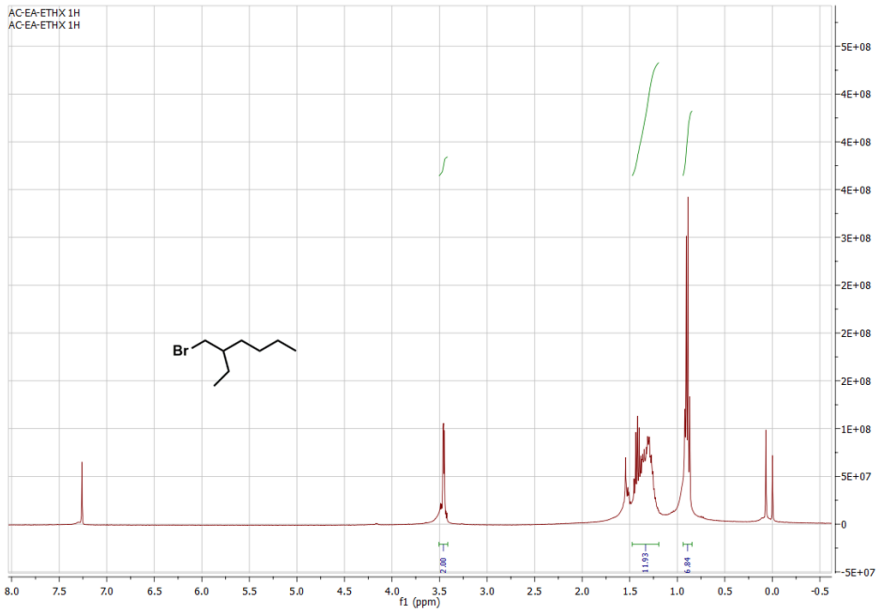

Figure 45. ^{1}H NMR result of 3-(bromomethyl)heptane

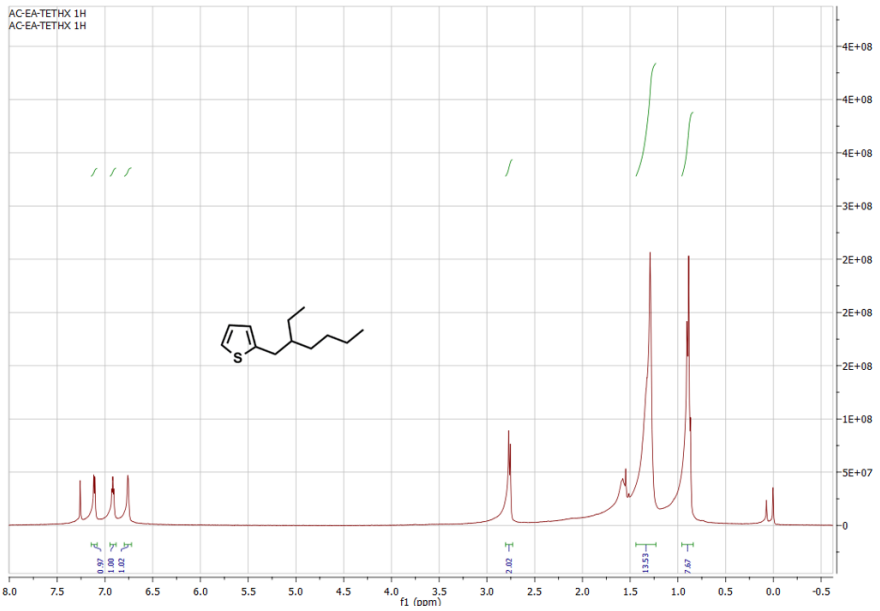

Figure 46. ^{1}H NMR result of 2-(2-ethylhexyl)thiophene

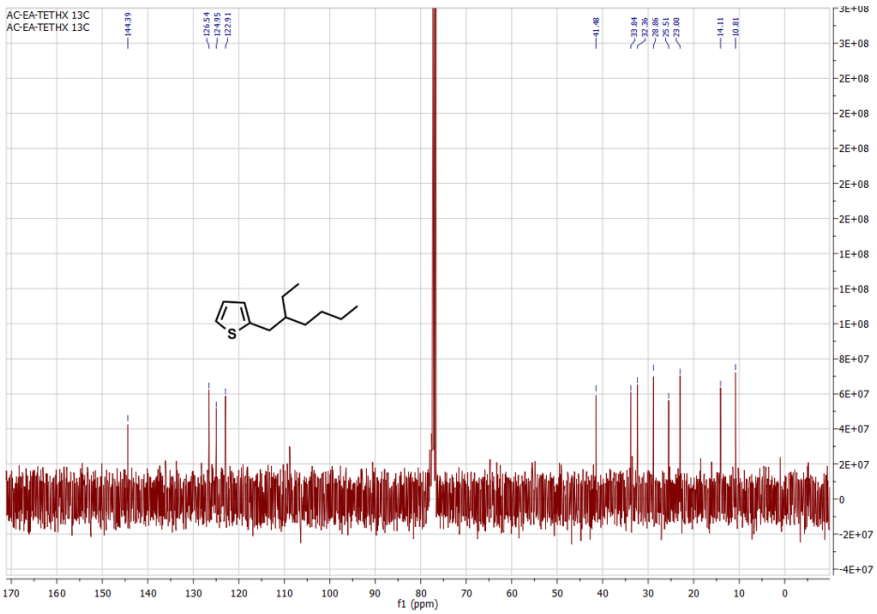

Figure 47. ^{13}C NMR result of 2-(2-ethylhexyl)thiophene

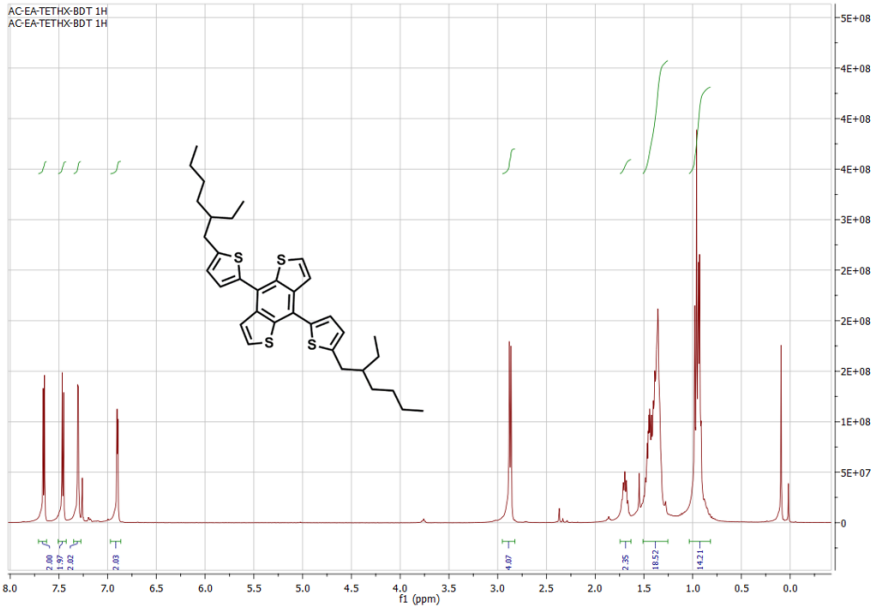

Figure 48. ^{1}H NMR result of 4,8-bis(5-(2-ethylhexyl)thiophen-2-yl)benzo[1,2-b:4,5-b']dithiophene

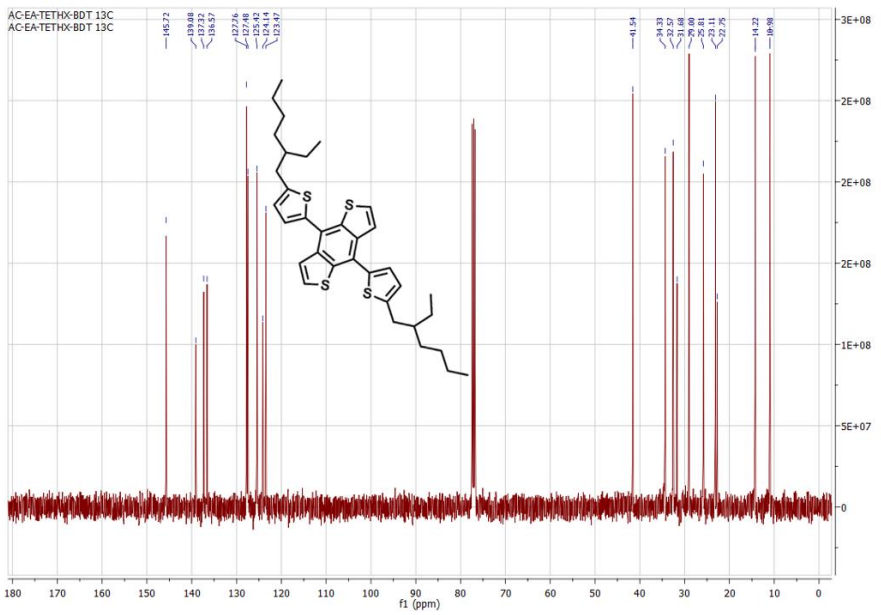

Figure 49. ^{13}C NMR result of 4,8-bis(5-(2-ethylhexyl)thiophen-2-yl)benzo[1,2-b:4,5-b']dithiophene

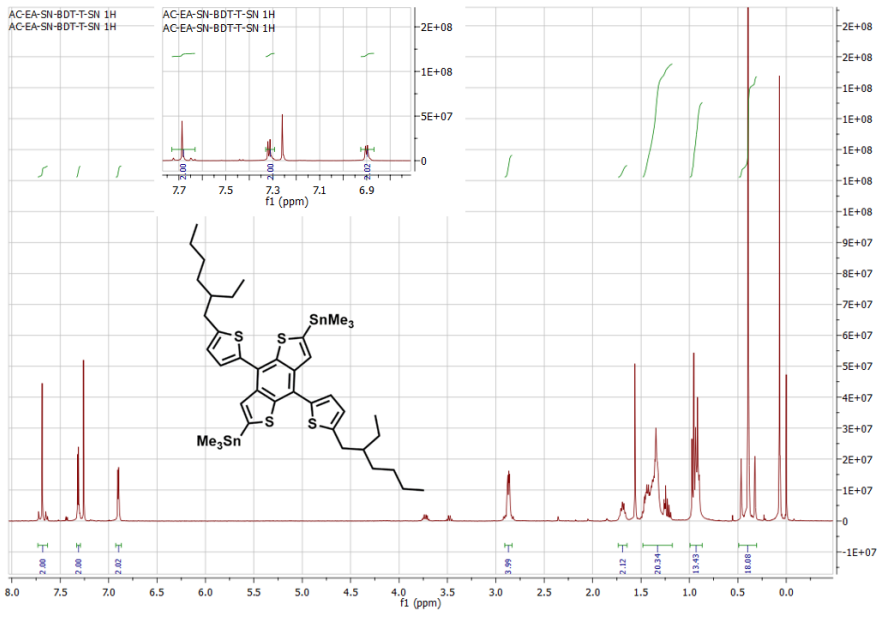

Figure 50. ^{1}H NMR result of 2,6-Bis(trimethyltin)-4,8-bis(5-(2-ethylhexyl)thiophen-2-yl)benzo[1,2-b:4,5-b']dithiophene

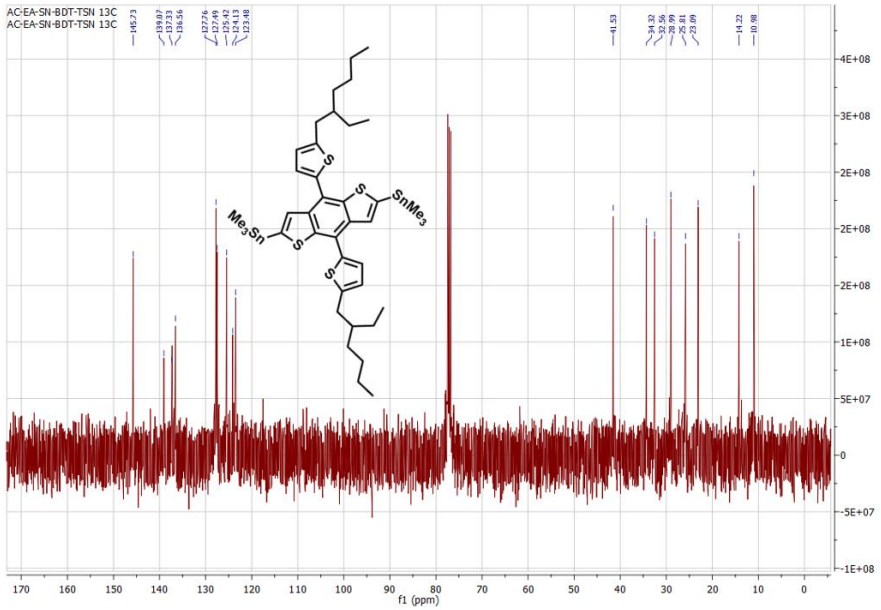

Figure 51. ^{13}C NMR result of 2,6-Bis(trimethyltin)-4,8-bis(5-(2-ethylhexyl)thiophen-2-yl)benzo[1,2-b:4,5-b']dithiophene

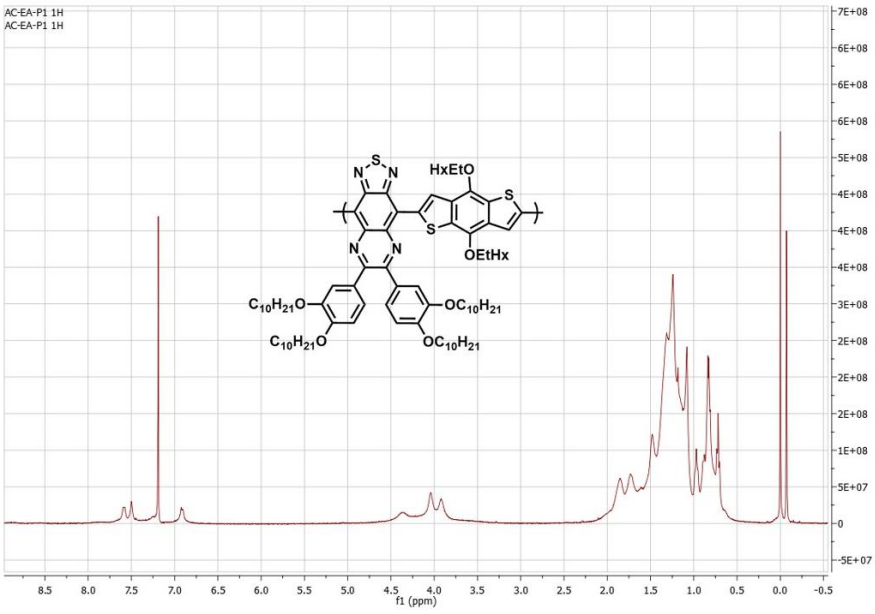

Figure 52. ^{1}H NMR result of **P1**

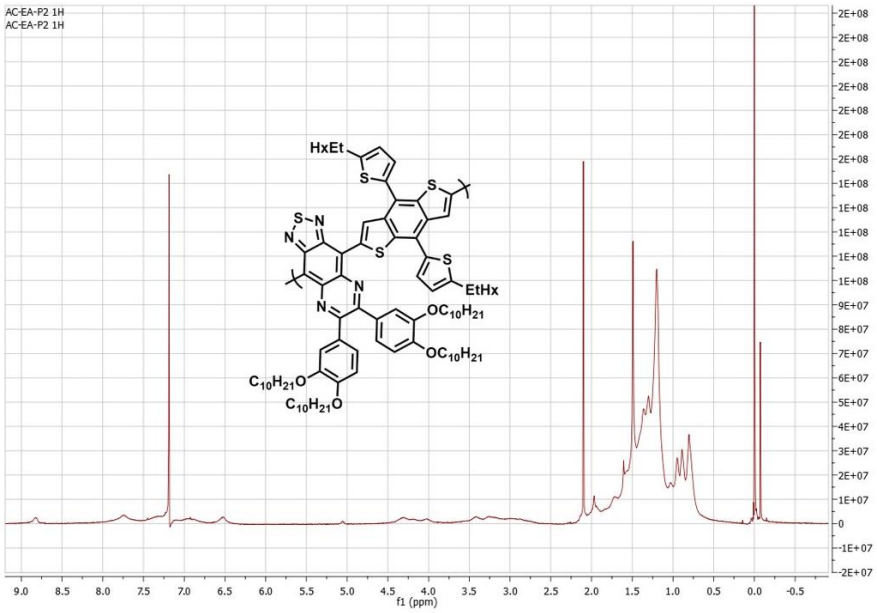

Figure 53. ^{1}H NMR result of **P2**

THERMAL ANALYSIS RESULTS

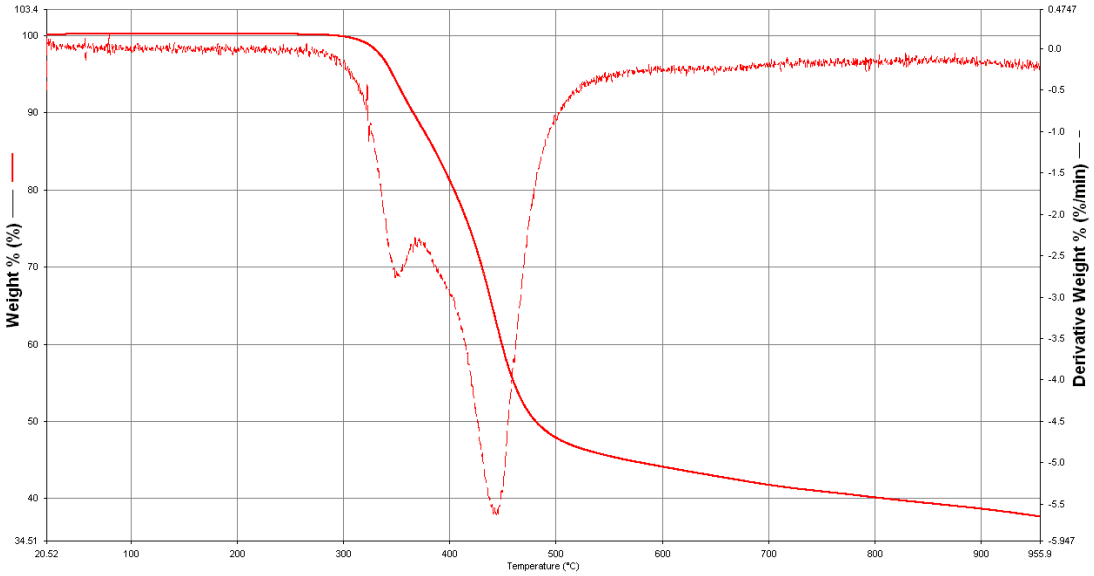

Figure 54. TGA result of **P1**

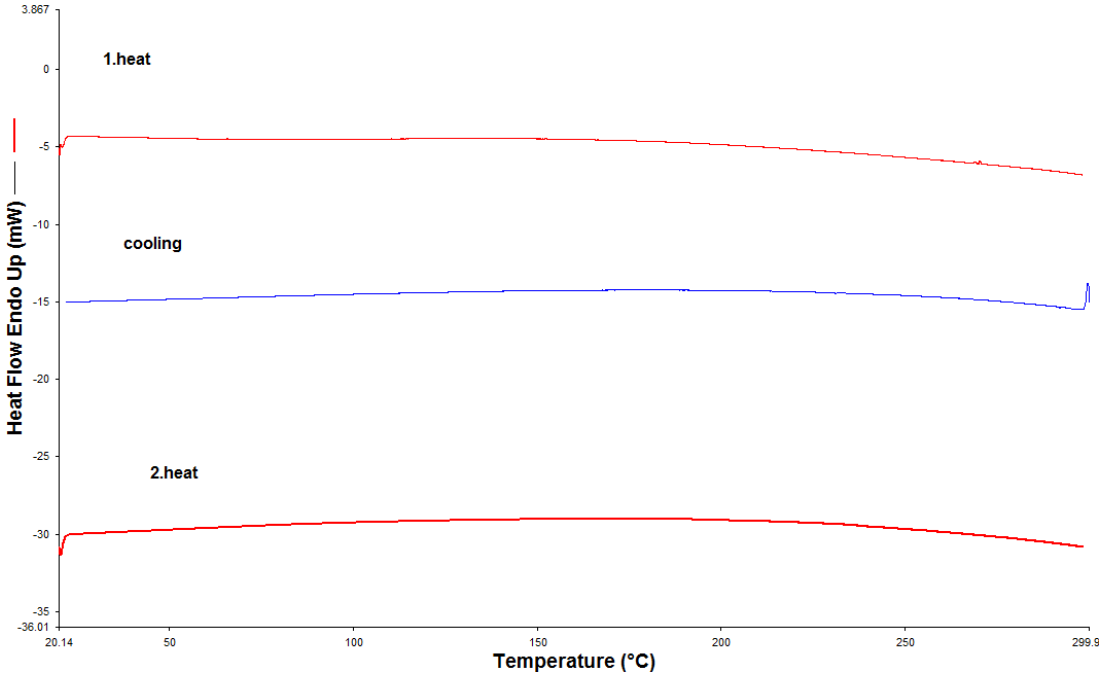

Figure 55. DSC result of **P1**

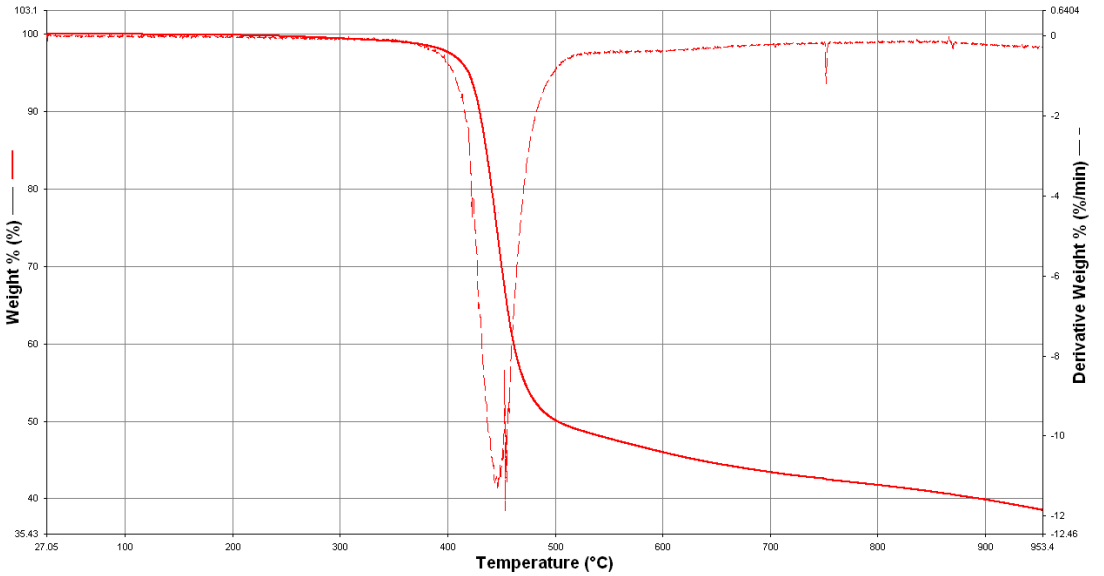

Figure 56. TGA result of **P2**

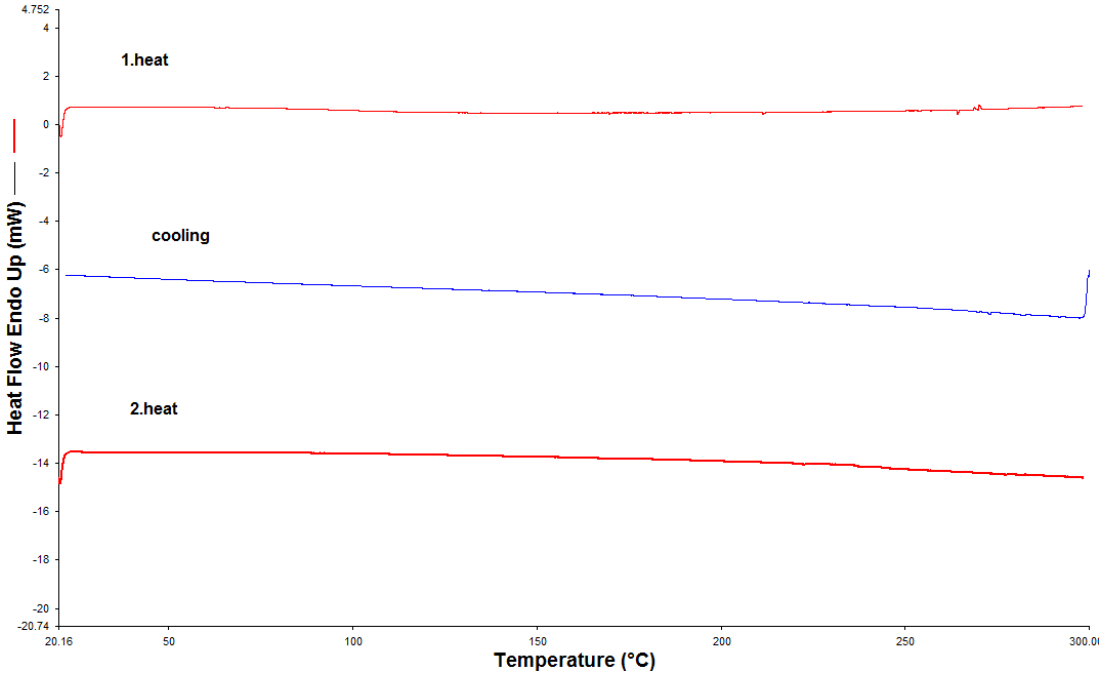

Figure 57. DSC result of **P2**